CRinc

THE UNIVERSITY of KANSAS CENTER for RESEARCH, INC.

2291 Irving Hill Drive-Campus West Lawrence, Kansas 66045

Progress Report for

A Research Program to Reduce Interior Noise
in General Aviation Airplanes

NASA Contract NCCI-6

STUDY OF THE DAMPING CHARACTERISTICS OF GENERAL AVIATION AIRCRAFT PANELS AND DEVELOPMENT OF COMPUTER PROGRAMS TO CALCULATE THE EFFECTIVENESS OF INTERIOR NOISE CONTROL TREATMENT

PART I

KU-FRL-417-19

Prepared by: R. Navaneethan

Jim Hunt

Brian Quayle

Approved by: Jan Roskam,
Principal Investigator

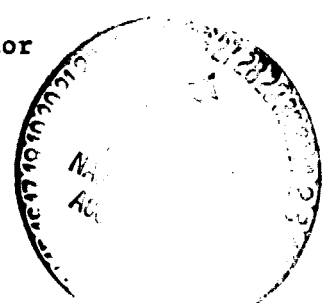

Flight Research Laboratory
University of Kansas Center for Research, Inc.
Lawrence, Kansas 66045

December 1982

SUMMARY

In this report, the work carried out at the University of Kansas Flight Research Laboratory (KU-FRL) to determine the damping characteristics of square, general aviation panels is presented. In addition, the progress on the work to date on the development of a simple interior noise level control program is also reported.

Structural damping plays an important role in the determination of noise reduction characteristics of panels. Since the damping varies considerably with different installations, it is not readily predicted. For this reason the investigation of the damping characteristics of panels installed in the KU-FRL test facility was undertaken. The tests were carried out on 20 x 20 inch panels at different test conditions. Tests were conducted on free-free panels, clamped panels, and panels as installed in the KU-FRL acoustic test facility. Tests with free-free panels verified the basic equipment set-up and test procedure. They also provided a basis for comparison.

The results indicate that the effect of installed panels is to increase the damping ratio at the same frequency. However, a direct comparison is not possible, as the fundamental frequency of a free-free panel differs from the resonance frequency of the panel when installed. The damping values of panels installed in the test facility are closer to the damping values obtained with fixed-fixed panels. Effects of damping tape, stiffeners, and bonded and riveted edge conditions were also investigated.

The noise reduction characteristics of a large number of general aviation aircraft panels have been investigated at this facility. An

attempt is now being made to calculate these characteristics analytically. For this purpose a well-known model to predict the transmission loss of the multilayered panels has been chosen. This model is being modified to include the effects of the experimental results obtained at the KU-FRL test facility. Skin, air gap, porous insulation blanket, septum, and trim panels are typical of the layers that are being considered. The agreement between the experimental results and the theoretical results obtained without any modifications to the program is generally poor. Several modifications and refinements are being made to the program to agree with the test results. The progress to date is also presented.

TABLE OF CONTENTS

TABLE OF CONTENTS (continued)

LIST OF FIGURES

LIST OF FIGURES (continued)

LIST OF TABLES

LIST OF SYMBOLS

Symbol	Definition	Dimension
a	Acceleration	[g]
a	Panel length	[m]
b	Panel width	[m]
b	Propagation constant	[nepers]
c	Damping coefficient	[Newton-sec/m]
c	Speed of sound	[m/sec]
C	Speed of sound	[m/sec]
d	Thickness of air gap or insulation	[m]
d	Distance	[m]
D	Flexural rigidity	[Nm]
D	Damping energy	[Nm]
E	Young's modulus	[N/m^2]
f	Frequency	[Hz]
h	Skin thickness	[m]
j	$\sqrt{-1}$	[-]
k	Slope factor (Equation 2.7)	[-]
m	Mass per unit area	[kg/m^2]
M	Mass per unit area	[kg/m^2]
n	Constant	[-]
n	Number of cycles	[-]
N	Number of layers	[-]
p	Pressure	[Pa]
P	Loads due to pressurization	[N]
Q	Quality factor (Equation 3.2)	[-]

LIST OF SYMBOLS (continued)

Symbol	Definition	Dimension
t	Time	[sec]
U	Elastic energy	[N, m]
x	Amplitude of oscillation	[m]
z	Impedance	[Rayls]
Z	Characteristics impedance	[Rayls]

Greek Symbol		
α	Absorption coefficient	[-]
δ	Logarithmic decrement	[-]
θ	Angle of incidence	[deg]
ζ	Damping ratio	[-]
ν	Poisson's ratio	[-]
η	Loss factor	[-]
ρ	Density of air	[kg/m^3]
ω	Angular frequency	[rad/sec]
τ	Transmission loss coefficient	[-]
ψ	Specific damping capacity (Equation 3.3)	[-]

Subscript	
ax	Axial
B	Air gap or insulation
C	Critical
cir	Circumferential

LIST OF SYMBOLS (continued)

Subscript	Definition
e	Base of natural logarithm (= 2.171828)
i	Integer
i	Incident
I	Incident
k	Integer
n	Fundamental resonance
p	Panel
r	Receiver
r	Reflected
t	Transmitted

LIST OF ABBREVIATIONS

Abbreviation	Definition
dB	Decibel
Hz	Hertz
KU-FRL	University of Kansas Flight Research Laboratory
NR	Noise reduction
RNG	Random noise generator
SEA	Statistical energy analysis
SLM	Sound level meter
SO	Sweep oscillator
TL	Transmission loss

CHAPTER 1

INTRODUCTION

This report is a continuation of the documentation of the research accomplished under continuing NASA Cooperative Agreement NCCI-6. The progress of the research accomplished during the period October 1, 1981, through March 31, 1982, was included in the previous report, KU-FRL-417-18 (Reference 1).

The present report covers the period from April 1, 1982, through October 31, 1982, of the current project year (May 1, 1982, through April 30, 1983). During this period, the Apple computer which was used in the data acquisition was stolen. Replacement of this computer by a cheaper H8 computer was time consuming and retarded the progress of the research in this report period. The H8 computer has now been integrated into the data analysis system. Also during this period, extensive calibration of the data acquisition system was carried out. One of the 1/4 inch microphones was found to make intermittent contact and was replaced by a 1/2 inch microphone. With this change, the results of the present tests became consistent with previous tests (see Reference 1 for problems on repeatability of tests at the KU-FRL test facility). The repeatability of the tests is good.

New concepts in noise attenuation, like panel treatments, depressurization, dual pane windows, and optimized multilayered structures, have been experimetally studies at various stages of this program. An attempt is being made to develop a simplified theory which will calculate the benefits in noise reduction that can be achieved with these

concepts. Chapter 2 discussed the computer programs so far developed to calculate the interior noise levels.

Panel damping is an important factor in the determination of noise reduction of panels. The boundary conditions of the panels also tend to play a significant role in the damping of the installed panel. For this reason damping of the panels, whose noise reduction characteristics have already been determined, was undertaken. The technique and the results are discussed in Chapter 3.

CHAPTER 2

DEVELOPMENT OF COMPUTER PROGRAM FOR THE DETERMINATION OF INTERIOR NOISE LEVEL

2.1 INTRODUCTION

The noise reduction characteristics of many general aviation panels have been experimentally investigated at the University of Kansas Flight Research Laboratory (KU-FRL) acoustic research facility (References 1-6). These include the bare and stiffened panel, dual pane windows, trim panels, damping material, and composite panels. The aim of the present study is to predict analytically the effect of these concepts on the interior noise level of general aviation aircraft. This is being done in two parts:

a. Development of a simple analytical model, which will "reasonably" predict the interior noise level inside the aircraft.

b. Modification of the analytical model to include the experimental results obtained at the KU-FRL acoustic research facility and the calculation of the interior noise level.

This report details the first part. The second part is still being done and will be the subject of a future report. The next section describes various interior noise control prediction methods. The method chosen is described in Section 2.3. The experimental noise reduction characteristics of three different panels are compared with the calculated values in Section 2.4. The discrepancies between the measured and the calculated results are due to various simplifications

and assumptions in the program and the characteristics of the KU-FRL acoustic test facility. No changes have been made in the program to account for these discrepancies. Section 2.5 describes the modifications done in the program to perform the sensitivity analysis of the important parameters of the noise control treatment design. Modification of the model to include the experimental results of the trim panels that are currently being used in the general aviation field is described in Section 2.6. Section 2.7 contains conclusions and the proposed changes in the program.

2.2 SURVEY OF METHODS FOR INTERIOR NOISE PREDICTION

The prediction of interior noise levels has attracted considerable attention during recent years. An excellent survey paper on the subject is Reference 7. A study of the current literature suggests that essentially four methods exist for analysis of sound transmission through a stiffened cylindrical shell, and only two of them include sound insulation and trim panel and other noise control treatments.

a. Classical Transmission Loss Approach: The extension of classical sound transmission theory to stiffened shells is presented in a series of papers by Professor Koval (References 8-12). This method relies heavily on the concepts of a locally reacting structural wall of infinite extent and its high frequency limit (Reference 7). The implementation for a typical aircraft noise control treatment is achieved through an extensive experimental study

of the insulation materials and empirical relations. Reference 13 initially derived the equations for the sound transmission through multilayered panels. Reference 14 extended the study to an actual aircraft structure. This method is also used in the two recent interior noise prediction models for the calculation of the effect of insulation and trim panels (References 15 and 16). As stated earlier, this method is valid in the "high" frequency limit and will not be accurate in the low frequency region.

b. Modal Methods: Since both the acoustic and structural models of the physical system can be represented in terms of mass, stiffness, and damping, the sound transmission through structures can be described in terms of structural and acoustic modes (References 16-20). The summation of individual modes is used to obtain the internal acoustic field resulting from structural motion (Reference 7). At high frequencies, summation is required over a large number of acoustic and structural modes, resulting in excessive computer time. However, at low frequency, when modal density is not excessive, this method is very attractive.

c. Statistical Energy Approach: The statistical energy analysis (SEA) bypasses the difficulties associated with detailed structural and acoustical models by using the average of large numbers of acoustic and/or structural modes (Reference 7). In this method the net inflowing acoustic power is cal-

culated and equated to net energy dissipation to obtain the interior levels (Reference 21). A study of the literature indicated that only the fuselage shell has been modelled by this method, and the other elements of a sound treatment scheme such as insulation and trim panel have not yet been included in the analysis. This method also has the severe handicap that it is applicable only in the frequency region where modal density is high. In this (i.e., high) frequency region, the effects of other elements of sound treatment cannot be neglected.

d. Band Limited Power Flow Approach: This method developed at the BBN (References 22-25) enables the use of power flow concepts at both low and high frequency regions. Beginning with modal analysis, a system of power flow and dissipation equations is written, encompassing the normal mode approach at low frequencies and statistical energy analysis at high frequencies (see Reference 25). This method has now been developed to include trim panel and sound insulation.

2.3 METHOD SELECTED

In choosing the method to be implemented at the KU-FRL, the following criteria were used.

a. The model should be simple and should incorporate various simplifications and assumptions to provide a reasonable engineering prediction tool.

b. Since the primary objective of this study is to compare the experimental results obtained on 18 x 18 inch panels with sound treatment, the method should have to account for the sound insulation, trim panels, etc.

c. The method should not require excessive computer time and memory and should be developed on the DIGITAL MINC-11 mini computer available at the Flight Research Lab.

The above criteria severely limited the choice of the analytical model. In the two recent interior noise prediction reports (References 15 and 16) for the high-speed propeller-driven aircraft, classical transmission loss equations initially developed by Cockburn and Jolly (Reference 14) were used to model add-on sound insulation. It was decided to use the same method at the KU-FRL. The model uses classical transmission loss theory. The entire noise control treatment is assumed to include skin (or the shell), air gaps, porous insulation material, septum, and trim panels. The noise reduction across the panel is assumed to be made up of transmission loss across this multi-layered panel and the absorption inside the cavity. At present it is being assumed that the cavity of the test facility is fully absorbent. The transmission loss of this panel is expressed in terms of the pressure ratio across each layer as

$$TL = 10 \text{ Log } \left| \frac{p_1}{p_2} \cdot \frac{p_2}{p_3} \cdots \frac{p_i}{p_{i+1}} \cdots \frac{p_N}{p_{N+1}} \right|^2 \qquad (2.1)$$

where TL = Transmission Loss across the panel

p_i/p_{i+1} = Pressure ratio across layer i

N = Number of layers.

The pressure ratio across each layer is calculated from the impedance of the layer and its terminating impedance. The model that is used for the shell (skin) is that of Koval (Reference 16). Mikulas' equation (Reference 15) can also be selected to calculate skin impedance. The equations developed in References 15 and 16 are used for the air gap and the porous materials. The septum is modelled as a limp panel. The trim panel can be modelled either as a limp panel (in case its mechanical properties such as Young's modulus, Poission's ratio, etc., are not known) or as a panel with single mode. In Appendix A the relevant equations used in the computer program are summarized.

2.4 COMPARISON WITH TEST RESULTS

The computer model was checked using sample inputs given in Reference 16. In this section the results from the model are compared with some of the test results obtained at the KU-FRL facility. No attempt has been made to modify the model. That will be done in the next phase.

2.4.1 Unstiffened Aluminum Panel

At the KU-FRL test facility an 18 x 18 x 0.32 inch panel is used as the standard panel; the results of other panels are normally compared with this panel. The noise reduction characteristics of this panel are shown in Figure 2.1. Also plotted are the results from the model. The discrepancy between the predicted and the measured values is due to the following:

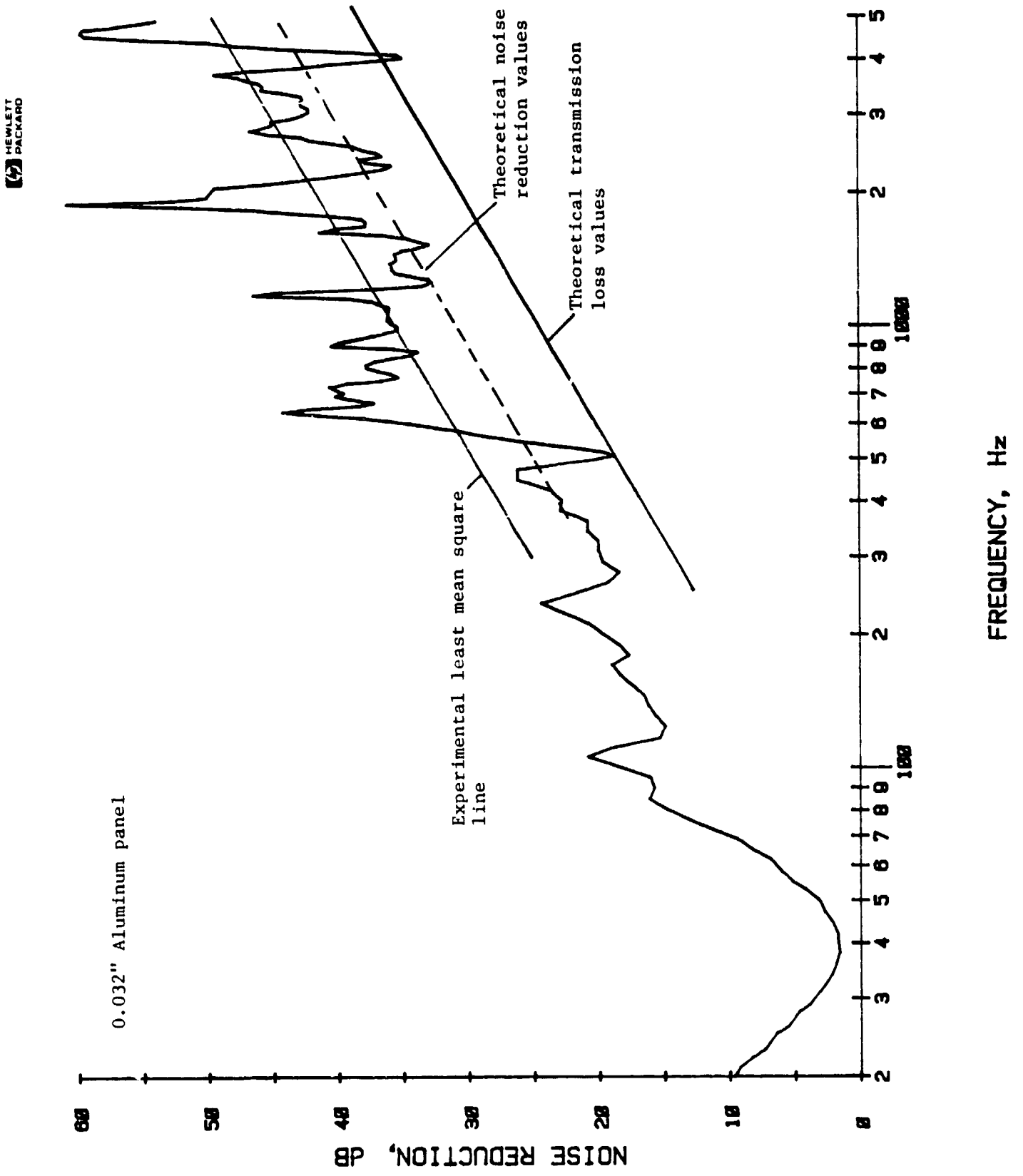

Figure 2.1: Comparison of Experimental and Theoretical Noise Reduction Characteristics of 0.032 Inch Thick Aluminum Panel

a. Because of the single mode assumption of the computer model, the resonance peaks and dips in the high frequency region are not predicted.

b. The computer model calculates the transmission loss defined by the relation:

$$TL = 10 \text{ Log } |(p_i/p_t)|^2 \qquad (2.2)$$

where p_i = Incident pressure

p_t = Transmitted pressure.

In the KU-FRL test facility it is not possible to measure incident pressure alone. The microphone measures the incident as well as the reflected pressures. The results from the KU-FRL give the noise reduction which is defined as

$$NR = 10 \text{ Log } |(p_i + p_r)/p_t|^2 \qquad (2.3)$$

where p_i = Incident pressure

p_r = Reflected pressure

p_t = Transmitted pressure.

For a simple mass law these two are related by (Reference 4)

$$TL = 20 \text{ Log } (1 + j\omega m/2\rho c)$$

$$NR = 20 \text{ Log } (1 + j\omega m/\rho c)$$

where $j = \sqrt{-1}$

ω = Circular frequency (radians/sec)

m = Mass per unit area

ρc = Impedance of air

ρ = Density of air

c = Speed of sound in air.

This gives, in the high frequency region, a difference of 6 dB. This line is also plotted on the same figure. The measured values are still higher by 4 dB. This is due to the characteristics of the test facility. However, the slope of the lease square line is very close to theoretical 6 dB/octave.

c. The computer model does not take into account the stiffening effect introduced by the receiver cavity. Hence the calculated fundamental resonance frequency is lower than the measured value. However, this stiffening effect is not predominant if the panel is inherently stiff. That is the case in most aircraft panels.

2.4.2 Stiffened Panel

The measured noise reduction characteristics of a stiffened flat aluminum panel (see Figure 2.2 for details of the panel) are shown in Figure 2.3. This figure is taken from Reference 3. The measured fundamental resonance frequency is 200 hz. At stiffness values corresponding to this resonance frequency the effects of the receiver cavity are negligible. The smeared stiffness model proposed in Reference 5 shows good agreement. The calculated values from the present computer program are shown in the same figure. This program predicts higher resonance frequency (220 hz) than measured value (200 hz). Once again the high frequency results agree with the least square values.

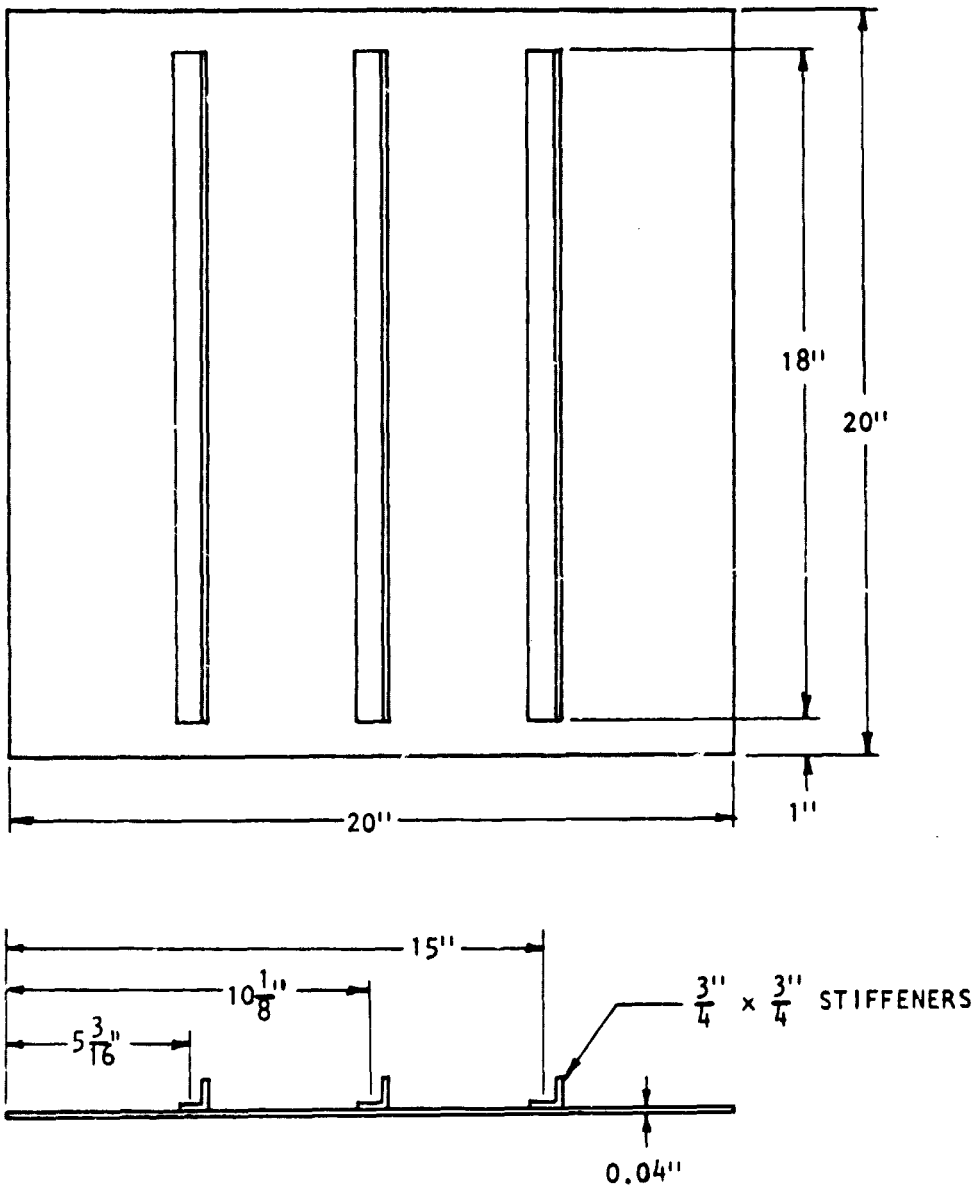

Figure 2.2: Details of the Stiffened Flat Aluminum Panel Tested at the KU-FRL Acoustic Test Facility

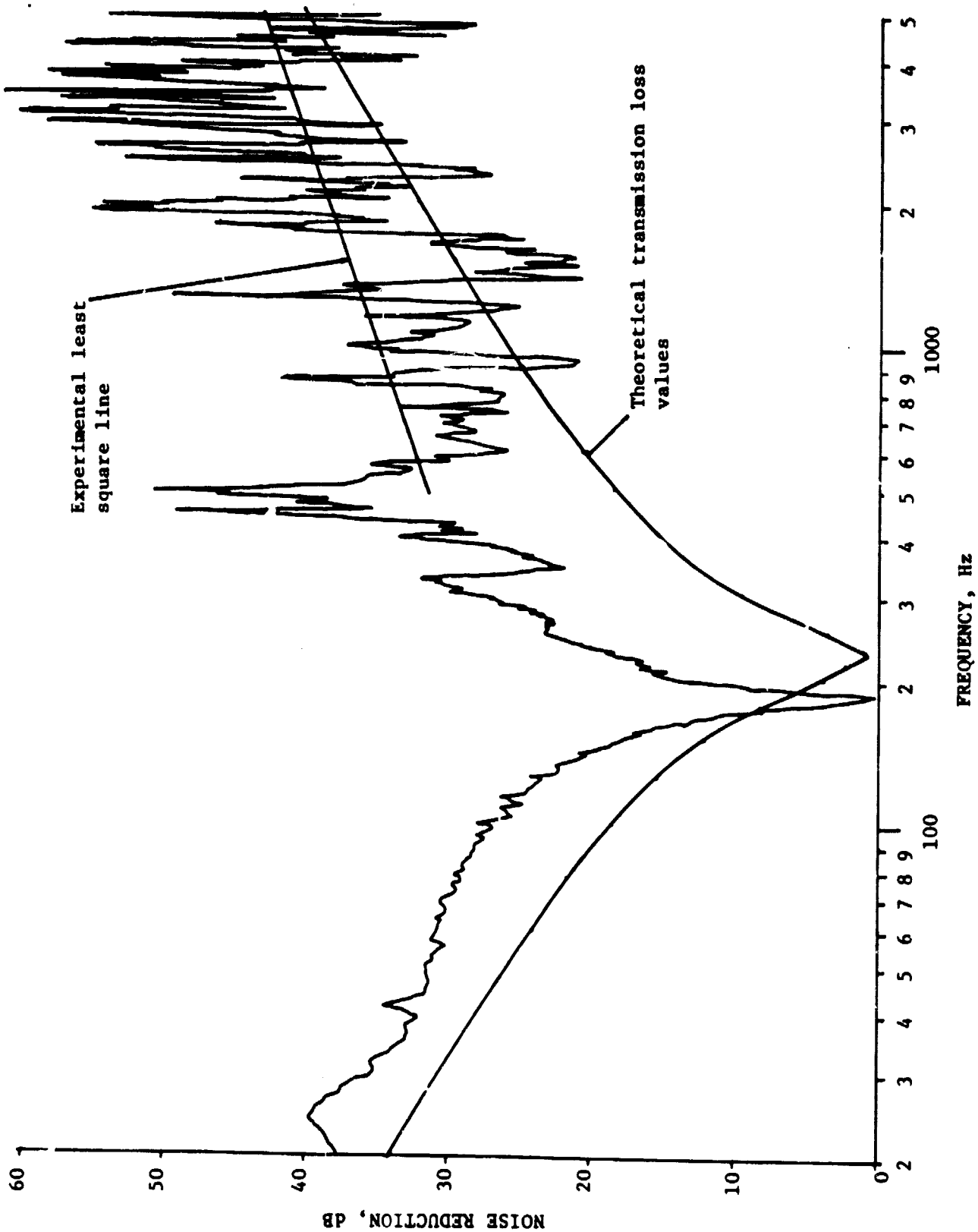

Figure 2.3: Comparison of Experimental and Theoretical Noise Reduction Characteristics of a Stiffened Aluminum Panel

2.4.3 Trim Panels

Normally the trim panels are made of some base material (Klegecell or Rohacell), and over that material some more trim material such as simulated leather, carpet, etc., is added. Normally these panels are modelled as limp panels, since the mechanical properties of these materials are not known. The computer program at KU can accept both limp panel impedance and the single-degree-of-freedom model impedance. To check the validity of the computer program, two panels available at the KU-FRL acoustic facility were selected; and noise reduction tests were carried out. Initially limp panel approximation was used. The predicted and measured values are compared in Figures 2.4 and 2.5. The panels tested were as follows:

a. 0.125 inch thick Klegecell type 75 with a layer of type A fiberglass on each side, plus an additional layer of .02 inch thick Royalite on one side;

b. 0.25 inch thick Rohacell with a layer of 120 phenolic prepreg skin on each side, plus an additional layer of .125 inch thick neoprene and woolen covering on one side.

In the limp panel model the stiffness effects of the Klegecell and the Rohacell materials are neglected. This gives lower noise reduction in the low frequency region. The effect of many layers in the trim panel is to increase the severity of the resonance peaks and dips. This lowers the least square average values of the high frequency noise reduction to well below the mass law values. The computer program does not model this effect.

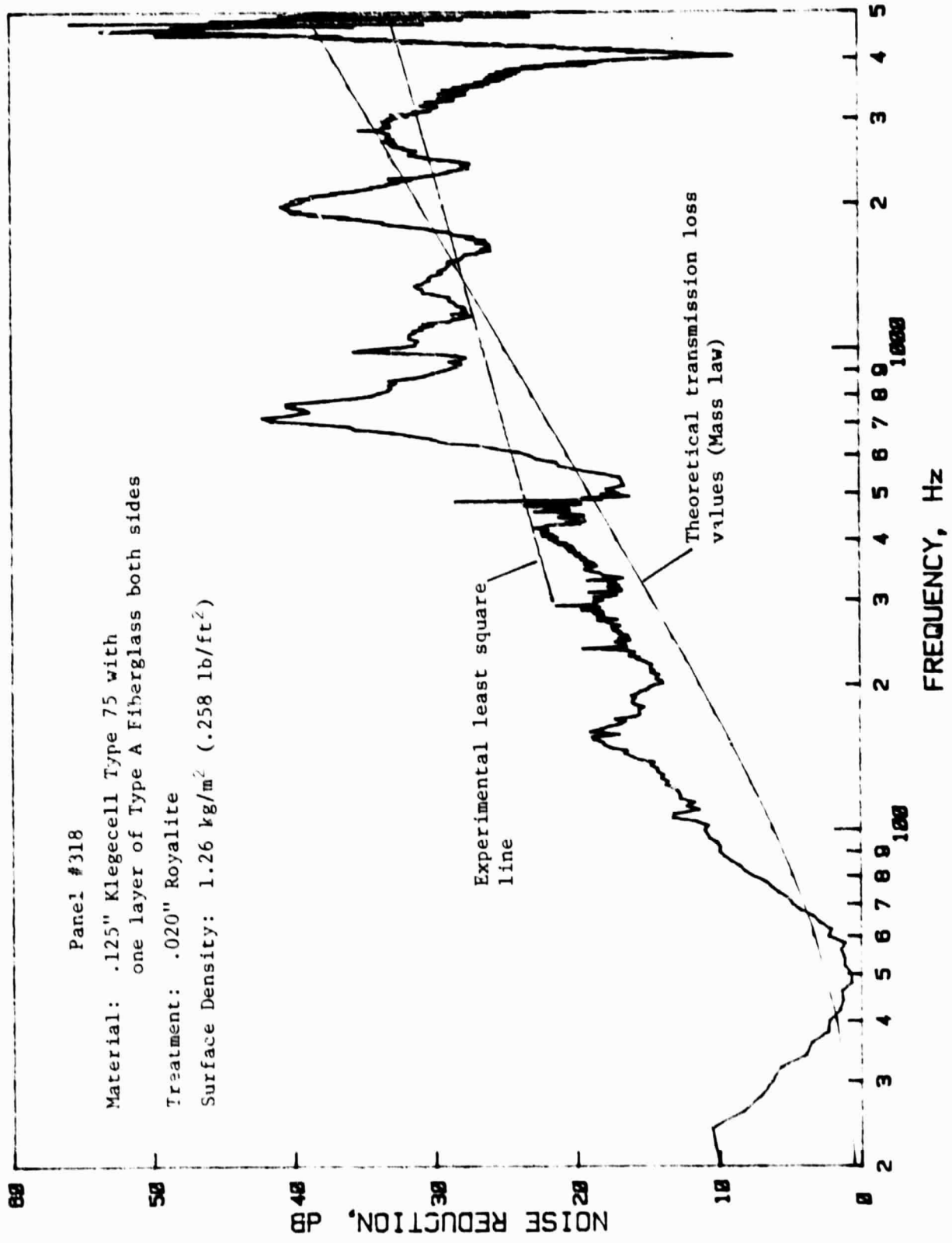

Figure 2.4: Experimental Noise Reduction Characteristics of Trim Panel #318

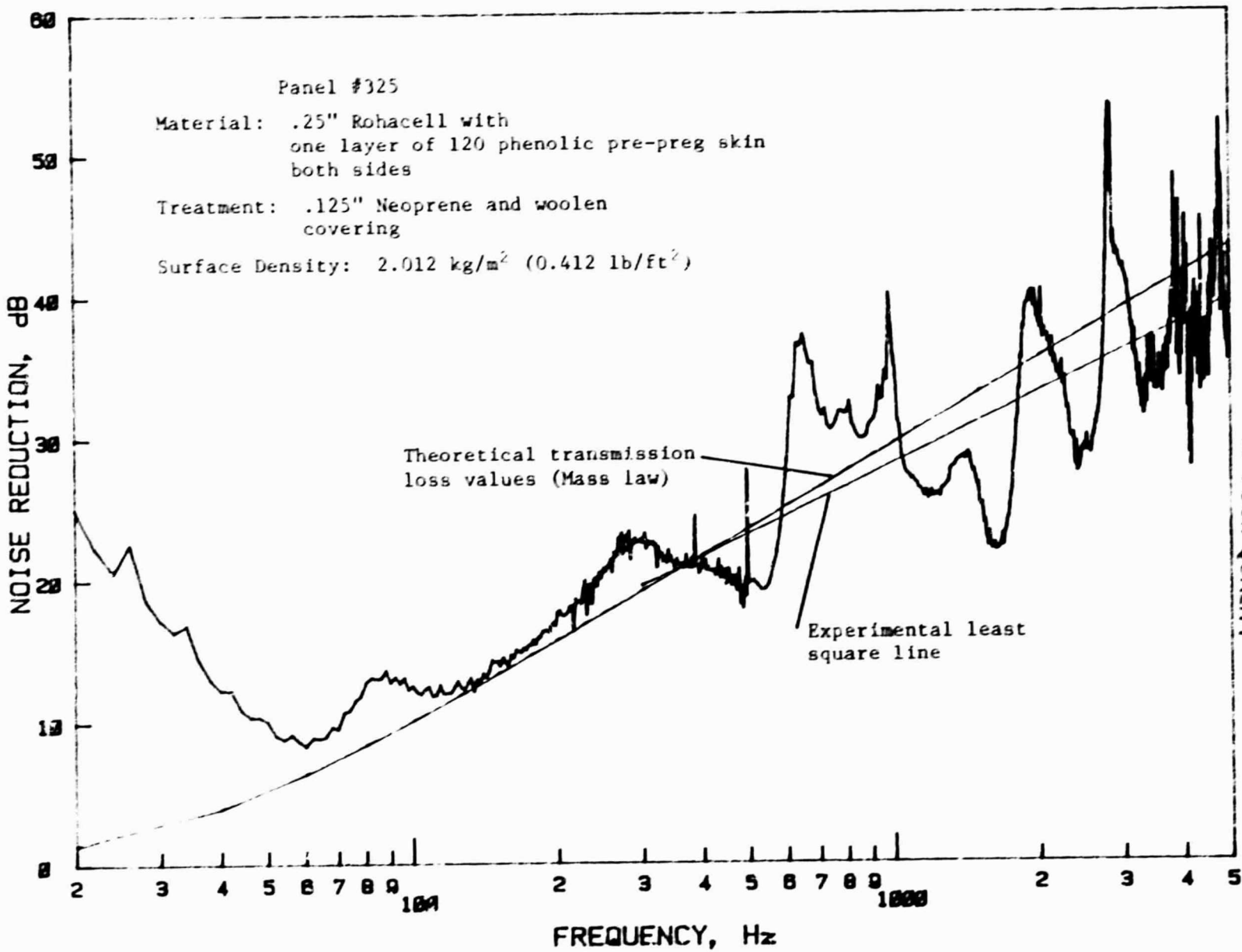

Figure 2.5: Experimental Noise Reduction Characteristics of Trim Panel #325

2.5 SENSITIVITY ANALYSIS

In general aviation aircraft design practice, interior noise control is seldom given any attention at the design stage. Noise control is designed after the fact. In such situations, knowledge of the sensitivity of the important noise control treatment parameters on the final noise reduction values is very helpful. This is especially true if the double wall resonance frequencies are close to the blade passage harmonics.

The computer model developed at the KU-FRL was modified to include this option. Air gap thickness, porous material thickness, septum surface densities, and the trim panel densities are considered the most important parameters in the noise control treatment. The program calculates the noise reduction values at 5 selected frequencies. The parameters are varied from half to twice the nominal values, and the trends are plotted for each of the five frequencies. Figures 2.6 through 2.8 show the sample output when using this option.

2.6 MODIFICATIONS FOR TRIM PANEL

The comparison of test results with the limp panel impedance approximation revealed the following two deficiencies in the model:

a. The limp panel approximation is seriously violated in the low frequency region due to stiffness effect of the trim panel base material. A completely theoretical single mode approximation requies the knowledge of the mechanical properties of these panels. These values are not normally known.

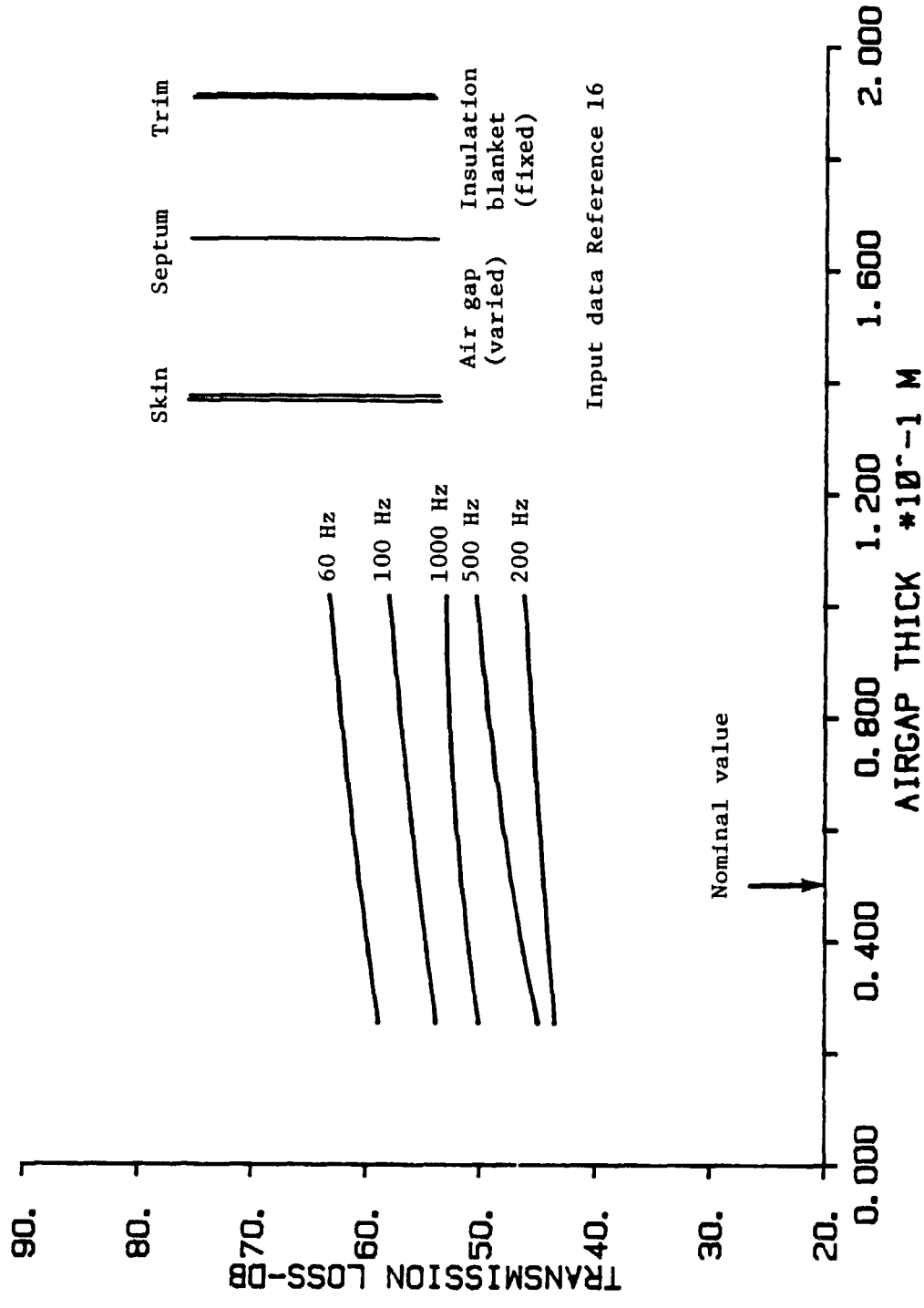

Figure 2.6: Sample Output: Effect of Varying Air Gap Thickness

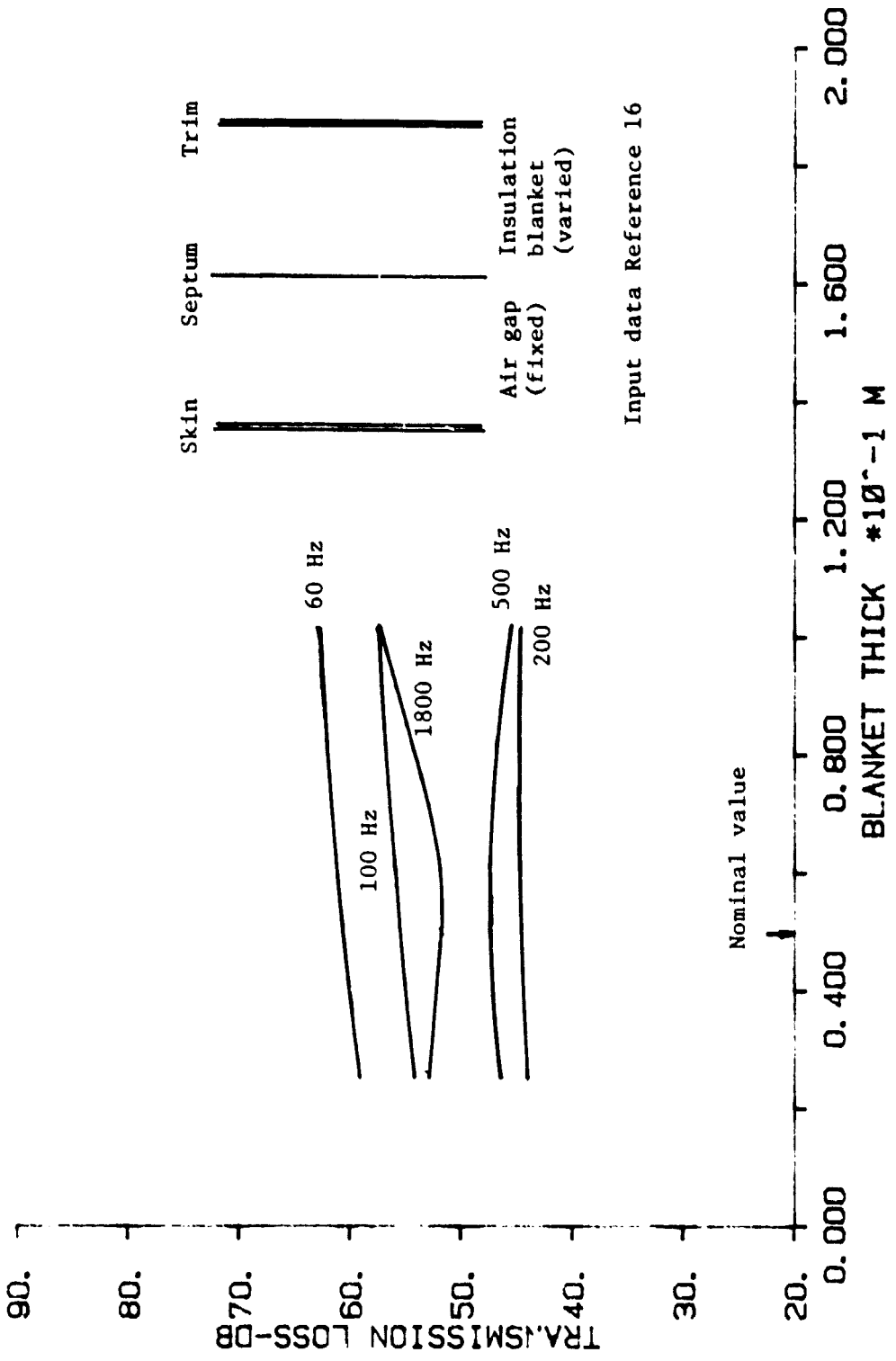

Figure 2.7: Sample Output: Effect of Varying Air Gap Thickness

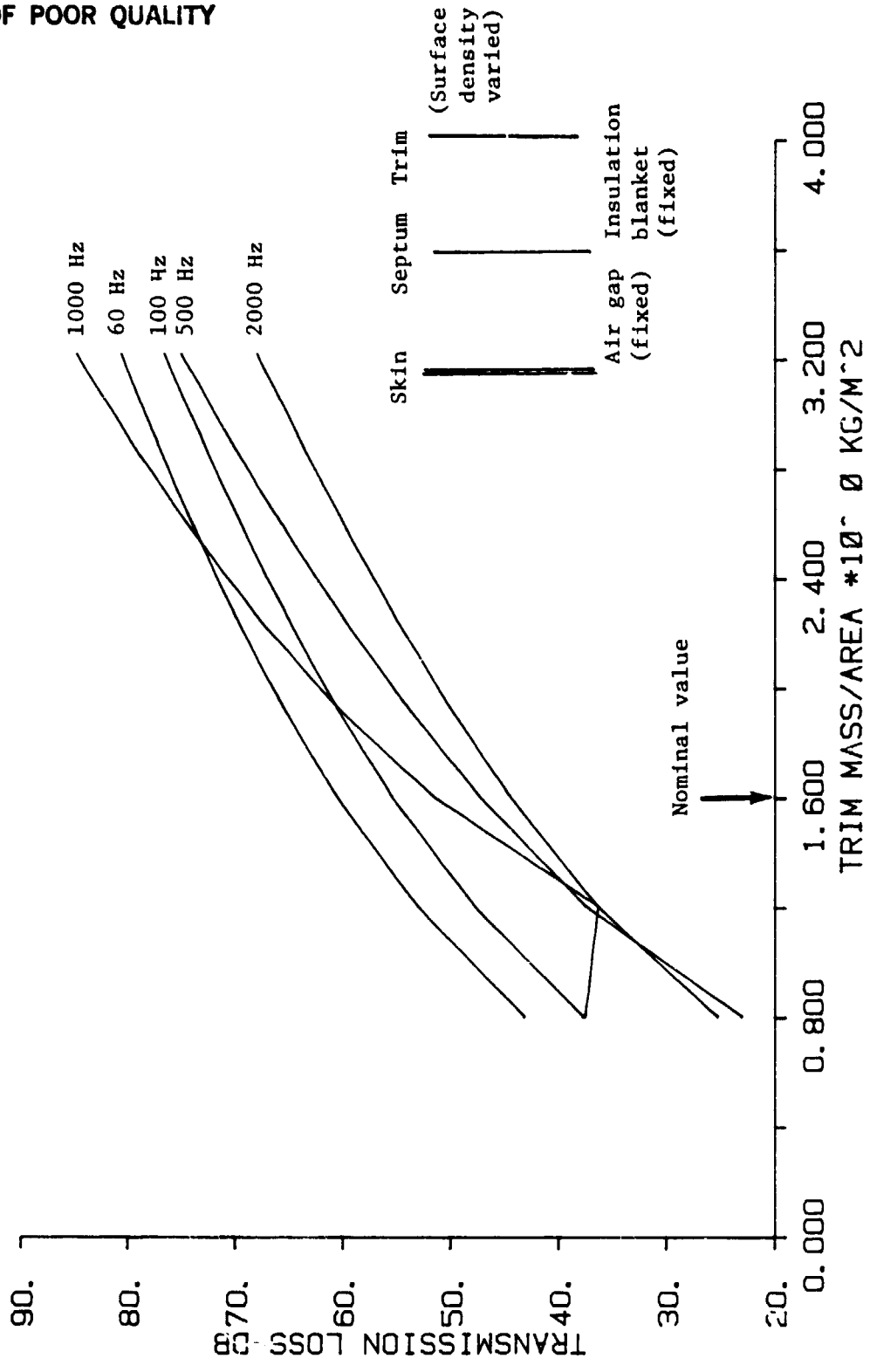

Figure 2.8: Sample Output: Effect of Varying Trim Panel Surface Density

b. In certain cases the measured values of the noise reduction in the high frequency region is far lower than the limp panel approximation, as can be seen from Figure 2.9. This figure is replotted from Reference 1. Also plotted on the same figure are the mass law values at the same frequency (i.e., 3000 hz).

The computer program has been modified to overcome these deficiencies. Reference 26 gives the single mode approximation for the panel impedance as

$$Z_p = 2\omega_n \zeta m + j\omega m[1 - (\frac{\omega_n}{\omega})^2] \tag{2.4}$$

where Z_p = Panel impedance

ζ = Damping ratio

ω = Circular frequency (= $2\pi f$)

f = Frequency

m = Mass per unit area of the trim panel

ω_n = Circular natural frquency (= $2\pi f_n$)

f_n = Natural frequency

$j = \sqrt{-1}$.

In the high frequency limit this becomes

$$Z_p = j\omega M \tag{2.5}$$

which is the usual mass law approximation. The measured fundamental resonance frequency and the damping ratio are used. A correction factor, k, called slope factor, is introduced to account for the difference in the high frequency region. With this factor the equation becomes

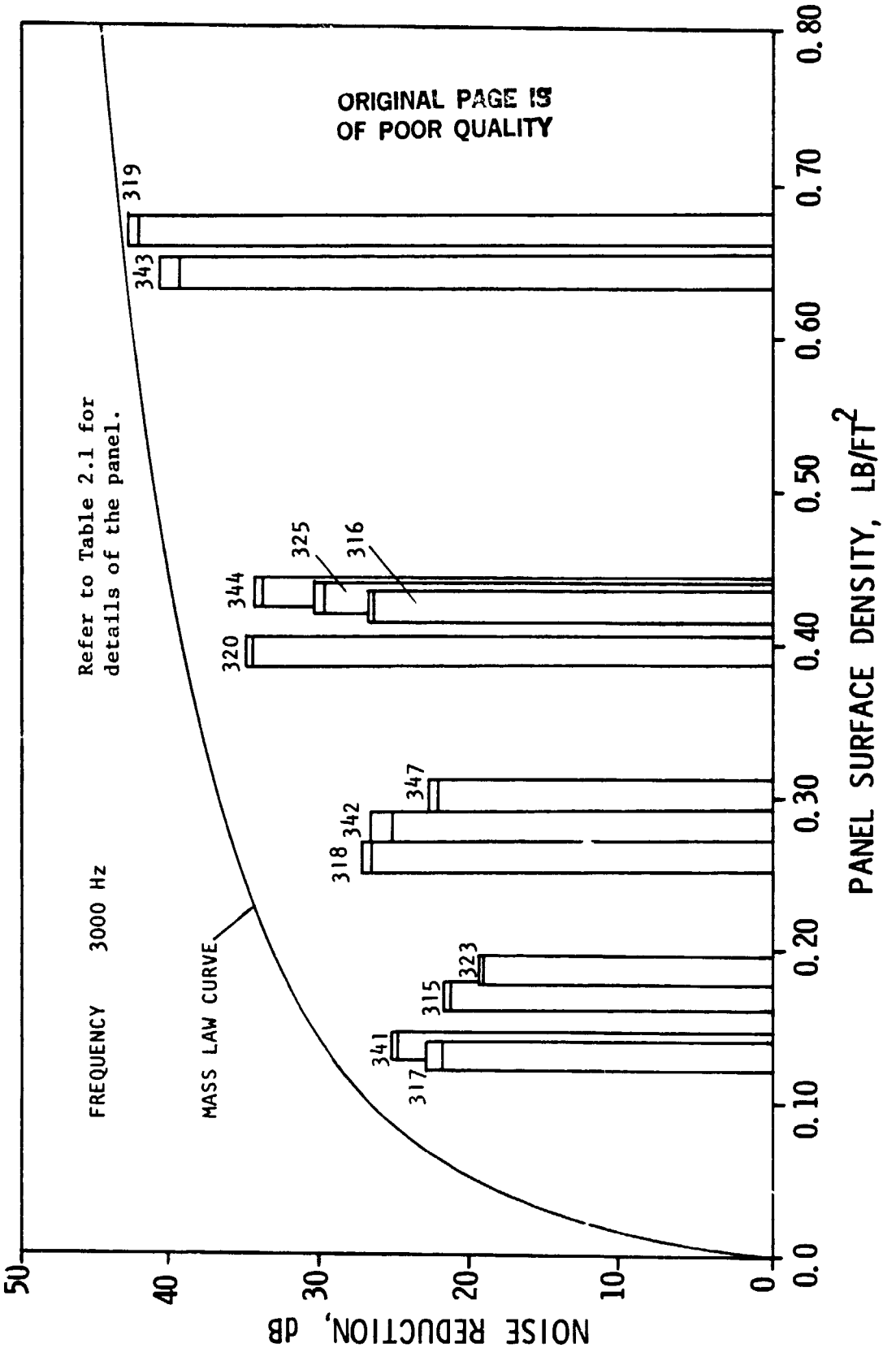

Figure 2.9: Comparison of Measured Noise Reduction of Various Trim Panels at 3000 Hz with the Calculated Values Using Mass Law

$$Z_p = 2\omega_n \zeta \omega m + j\omega mk[1 - (\frac{\omega_n}{\omega})^2]. \quad (2.6)$$

The factor k is given by

k = measured increase in dB per octave/6 dB per octave.

For all the trim panels tested at the KU-FRL acoustic test facility, the fundamental resonance frequency and the slope of the least square lines were measured directly from the noise reduction results. The damping ratio at the resonance frequency was measured using the technique described in Chapter 3. These values are tabulated in Table 2.1. The results of the computer program for the same two panels discussed in Section 2.4.3 are plotted in Figures 2.10 and 2.11. This has considerably improved the prediction of the noise reduction characteristics of the trim panel.

2.7 CONCLUSIONS

A series of simple computer programs have been developed within the restrictions of the computer memory and running time. The agreement with the experimental values was not good. This is because of both the simplicity of the theoretical model and the characteristics of the KU-FRL acoustic test facility. Further refinements to the model are required before it can be used to explain the results obtained from the KU-FRL acoustic test facility and to predict actual aircraft interior noise reductions.

Table 2.1 Details of the Trim Panels Tested at the KU-FRL Acoustic Test Facility

Panel	Material	Treatment	Measured Resonance Frequency	Measured Mass per Unit Area	Measured Damping Ratio	Measured* Slope Factor
			Hz	(kg/m^2)		
315	0.25" Klegecell with 1 layer type A fiberglass	-	150	0.82	0.0717	0.35
316	(same as above)	0.125" neoprene + wool covering	100	2.06	-	0.45
317	0.125" Klegecell with 1 layer type A fiberglass	-	100	0.62	0.0712	0.33
318	(same as above)	0.020" Royalite covering	50	1.26	0.0647	0.53
319	(same as above)	carpet	42	1.07	-	0.61
320	(same as above)	0.5 inch foam + simulated leather covering	68	1.93	-	0.45
323	0.25" Rohacell with 1 layer 120 phenolic pre-preg skin	-	160	2.09	0.0721	0.30
325	(same as above)	0.125 neoprene + wool covering	60	2.09	0.0738	0.83
347	(same with 2 layers 120 phenolic skin)	-	175	1.47	0.0605	0.33
341	0.125" Rohacell with 1 layer 120 phenolic skin	-	68	0.65	0.0696	0.35
342	(same as above)	0.020" Royalite	90	1.36	0.0606	0.40
343	(same as above)	0.5 inch carpet	50	3.29	0.0604	0.61
344	(same as above)	0.25" neoprene + leather covering	65	2.11	0.0563	0.51

*Measured slope factor = (measured slope)/6

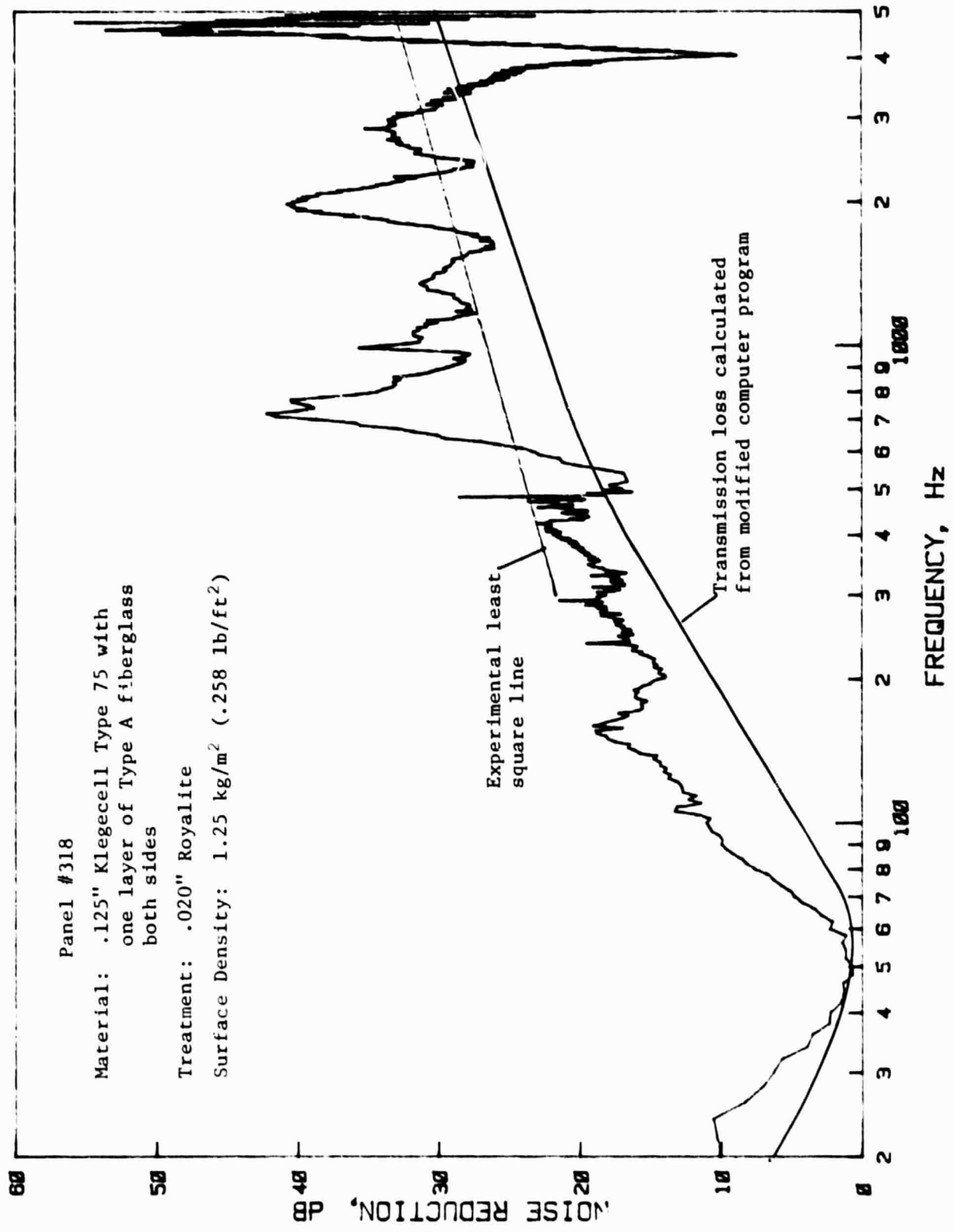

Figure 2.10: Noise Reduction Characteristics of Trim Panel #318, Calculated from Modified Computer Program

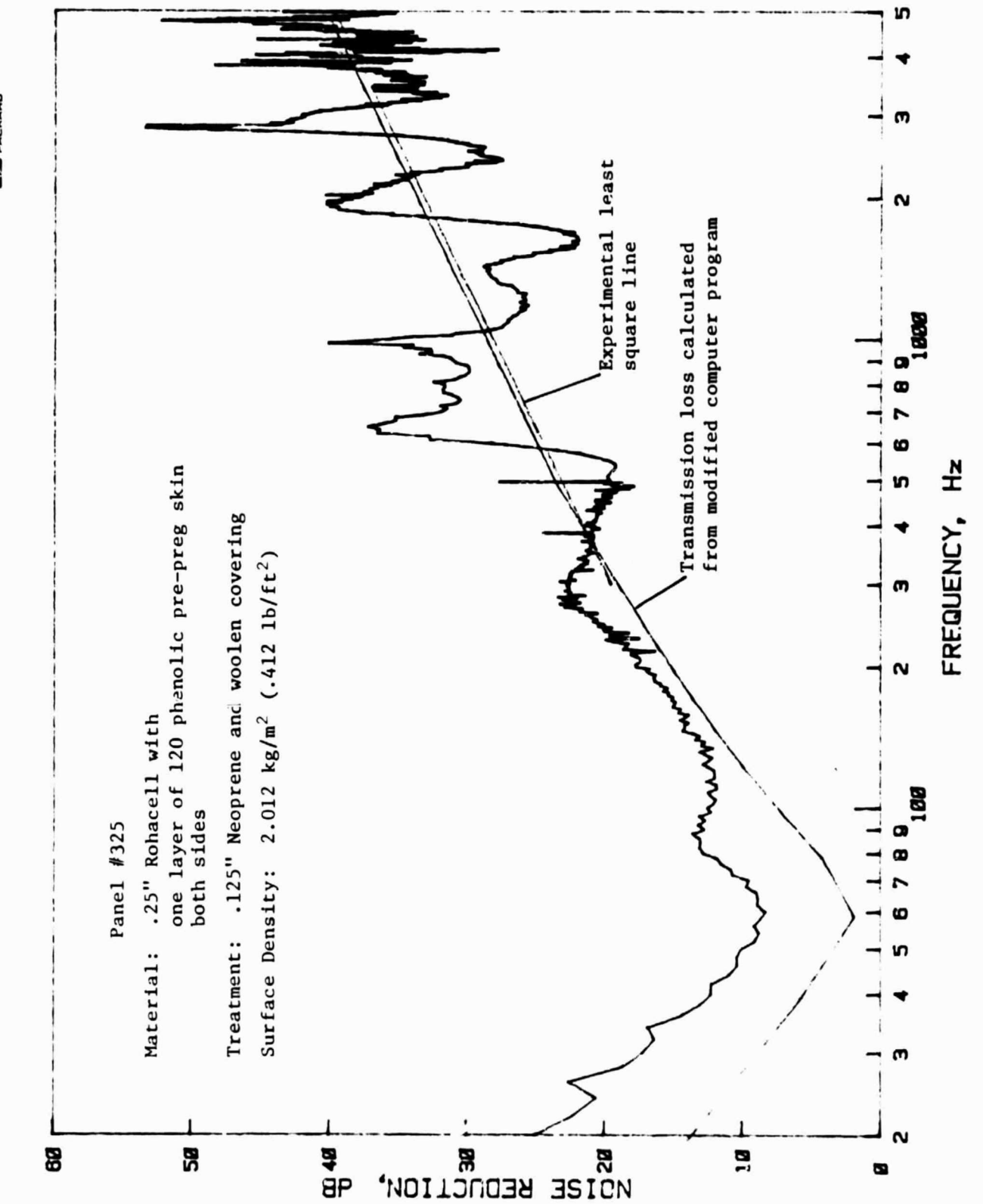

Figure 2.11: Noise Reduction Characteristics of Trim Panel #325, Calculated from Modified Computer Program

CHAPTER 3

DETERMINATION OF LOSS FACTORS

3.1 INTRODUCTION

This test program has been conducted in the KU-FRL acoustic test facility to determine the damping of panels mounted in the Beranek tube. Damping is defined as energy dissipation of a structure as it deforms and the conversion of ordered mechanical energy into thermal energy. Unlike mass and stiffness, damping does not refer to a unique physical phenomenon; and that is the reason damping is so much more difficult to predict in general. Damping mechanisms include interface friction, acoustic radiation, magnetic hysteresis, mechanical hysteresis (also called material damping), and any other way of converting mechanical into thermal energy. In practical cases one or two mechanisms generally predominate (Reference 27). For example, the material damping in aluminum alloy structures is known to contribute only a tiny proportion to the total damping (Reference 28). Likewise magnetic hysteresis has a very small effect.

The panel damping is an important factor for noise reduction at the fundamental frequency and also in the mass law region (higher frequencies). Damping in panels is very dependent on the particular mode; as a result, the boundary conditions of the panel play a significant role in the damping of the installed panel (Reference 29). Since the damping varies considerably with different installations, it is not readily predicted. For this reason, this evaluation of a technique for the determination of the damping in panels in this facility was undertaken.

This chapter details the equipment and the method used to obtain the required data and the techniques for reducing the data to usable terms. Also described are the tests used to validate the results obtained for the panels installed in this facility, and the conslusions reached as a result of these tests are presented. Appendix C contains a section describing the methods used to install the accelerometer on the panels.

3.2 DEFINITION OF TERMS

There are many units and terms used for designating damping in materials. Of these the loss coefficient, η (or loss factor, as it is commonly called) is often used in structural mechanics and will be used in this paper. Loss coefficient is a relative energy unit defined as the ratio of damping energy to strain energy and is applicable to both linear and nonlinear materials.

$$\eta_s = D_s/2U \tag{3.1}$$

where D_s is the damping energy dissipated in the total specimen

U_s is the total elastic energy stored in the specimen.

The subscript s denotes that these values are specimen properties. These properties are dependent on the specimen configuration as well as the material properties. This subscript will be dropped subsequently with the understanding that all values for η are specimen loss factors.

For purposes of comparison of results with those of other investigators, the relations with several other common measures of damping are given below.

1. Quality factor, Q: Physically this is amplification at resonance.

$$Q = 2\pi U/D = 1/\eta \tag{3.2}$$

2. Specific damping capacity, ψ

$$\psi = D/U = 2\pi\eta \tag{3.3}$$

3. Damping ratio, ζ: Fraction of critical damping.

$$\zeta = C/C_c = \eta/2 \tag{3.4}$$

C is the viscous damping coefficient, lbf-sec/in

C_c is the critical damping coefficient, lbf-sec/in

4. Logarithmic decrement, δ

$$\delta = \ln(x_o/x_1) = \pi\eta \tag{3.5}$$

x_o = the amplitude of the damped wave at point 0.

x_1 = the amplitude of the following wave after 1 cycle.

For further explanation of measures and nomenclature of damping, see References 27, 30, 31, 32, and 33.

3.3 TECHNIQUES FOR DAMPING EVALUATION

Several methods have been used to determine the damping of a specimen. Those that can be applied to a panel include bandwidth, energy measurements, amplification factor, and decay rate.

For the bandwidth method a frequency sweep is made, and the bandwidth is measured at a specified fraction of maximum amplitude. Problems arise when modes are closely spaced, as is the case with most panels for all but the first one or two modes.

The energy measurement method involves directly measuring the energy input (amplitude and phase) and the specimen output (amplitude and phase) and using these to calculate the energy loss directly. This requires more elaborate and expensive equipment.

Measurement of amplification factor is difficult to use for absolute measurement of damping, since the reference level may be hard to find.

Decay rate or logarithmic decrement tests are easy to do and are widely used. Here the excitation force is turned off and the panel is allowed to vibrate freely with the response, as measured by a vibration pickup, recorded. The logarithmic decrement, δ, can then be obtained from this record using the relation $\delta = \ln(x_0/x_1)$. The limitation on this method is the assumption that the decay curve is logarithmic. Physically this means that δ must be independent of amplitude (viscous damping). When this assumption is violated (the curve is not logarithmic), a logarithmic curve can be fitted to the decay curve and an equivalent value for δ can be found. Because of the simplicity and reliability of this method, the damping values will be determined using the decay rate tests.

3.4 EQUIPMENT

The equipment set-up for the decay rate tests is shown in Figure 3.1. The panel displacement can be measured by several devices, including capacitance pickups, accelerometers, or lasers. An accelerometer was chosen over the capacitance pickup because of the ease of

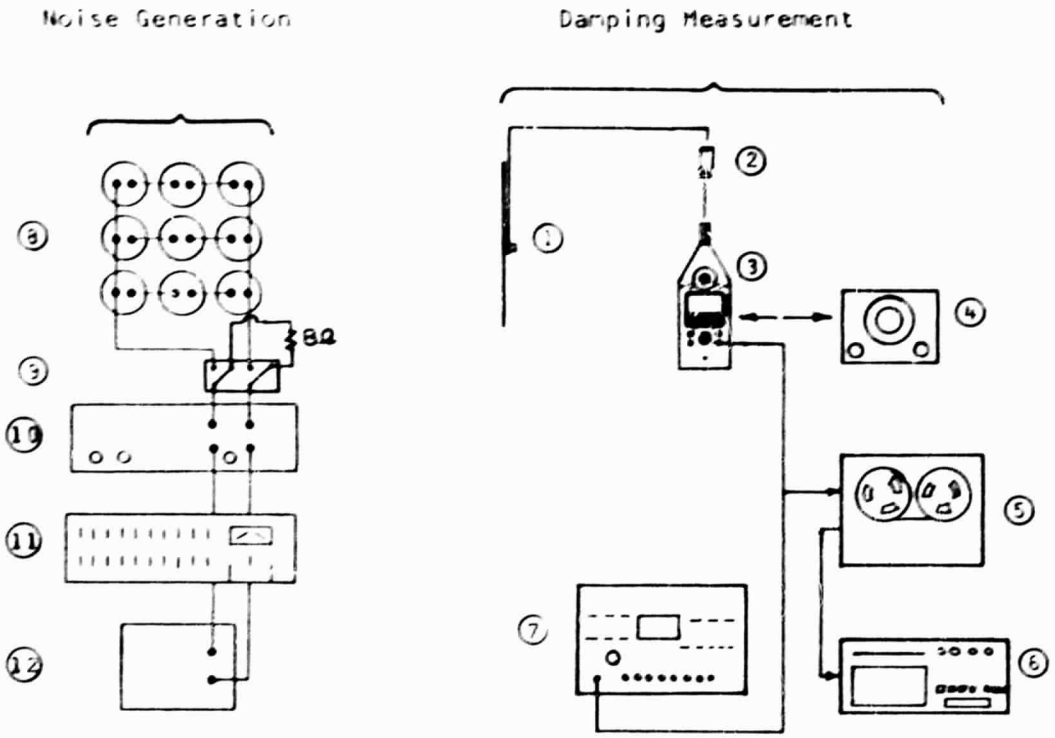

1 - B&K Accelerometer Type 4344
2 - B&K Integrator Type ZR0020
3 - B&K Sound Level Meter
Type 2209
4 - Filter
a) B&K Third-Octave
Filter Set Type 1616
b) Multimetrics Industries
Model AF-120 Active Filter
5 - Magra SJS Tape Recorder
6 - Recorder
a) Honewell Visicorder Oscillograph
Model 1508C
b) Techni-rite Dual Channel
High Speed Recorder Model TR722
7 - Spectral Dynamics Model SD335
Real Time Analyzer
8 - Altec 405-8G Speakers
9 - Single-throw Double-pole Switch
10 - Crown D-150 Power Amplifier
11 - TAPCO 2200 Equalizer
12 - Noise Source
a) General Radio 1390-A
Random Noise Generator
b) HP 3300A Function
Generator

Figure 3.1: Equipment Set-up for Noise Generation and Damping Measurements

installation and operation. Since the mass of the accelerometer is very small, the loading on the panel is insignificant, as shown in the next section. The integrator on the sound level meter (SLM) has a switch to select output of acceleration, velocity, or displacement. The active filter (4b)*was used when the third octave filter (4a) was out of service. A comparison test run with each filter yielded the same results for each. For the first tests the Techni-rite hot stylus recorder (6b) was used with a capability of recording up to 125 Hz and 100 mm/sec. This was inadequate for the modes above the first; so the Honeywell oscillograph (6a), with a capability of recording up to 1000 Hz and 80 inches per second, was used for all subsequent tests. The sweep oscillator (SO; 12b) was chosen over a random noise generator (RNG; 12a) because tests with the RNG produced nonanalyzable results.

A switch was installed in the wires between the amplifier and the speakers, as shown in Figure 3.1. This single throw switch diverts the current to an 8Ω to prevent damage to the amplifier when the speakers are shut off for the decay tests.

3.5 TEST METHOD

The most important factor to consider in damping testing is to test the specimen in a configuration which bears a close resemblance to the application of the results. For this reason the damping will be evaluated with the panel in the same installation used for the noise reduction tests.

---

*Figures within the parentheses denote equipment described in Figure 3.1.

3.5.1 Panel Installed in Beranek Tube

For the decay rate tests the accelerometer was mounted on the panel as described in Appendix C. For the first few tests the accelerometers were mounted with the cement, but for later tests bee's wax was used because of the ease of installation and removal and the slightly improved performance reported in Reference 34. The accelerometer cable was routed toward the top of the panel and taped with electrical tape at three points to minimize triboelectric noise caused by vibration of the cable. The panel was then placed in the Beranek tube (Figure 3.2), and the 8 clamping bolts were torqued to 25 in-lb. After connecting the accelerometer cable to the sound level meter (SLM) and sending the AC output to the spectrum analyzer, a frequency sweep was run from 20 Hz to 1000 Hz to locate the resonant peaks for the panel. This frequency response was then stored on the Spectrascope, and the AC output of the SLM was connected to the tape recorder for signal amplification. The amplified signal was then sent to the oscillograph.

For the actual tests the first resonant peak was located on the scope and the frequency read. This frequency was then tuned on the oscillator and minor adjustments made to yield the maximum acceleration as indicated on the SLM. This peak does not necessarily correspond to the resonant frequency of a specific mode, but for small damping it is extremely close. Acceleration was used as output, since the displacements were so small that the meter was operating at its lower limits for even the low frequencies and was mostly noise at the higher frequencies. The gain on the recorder was then adjusted to yield the

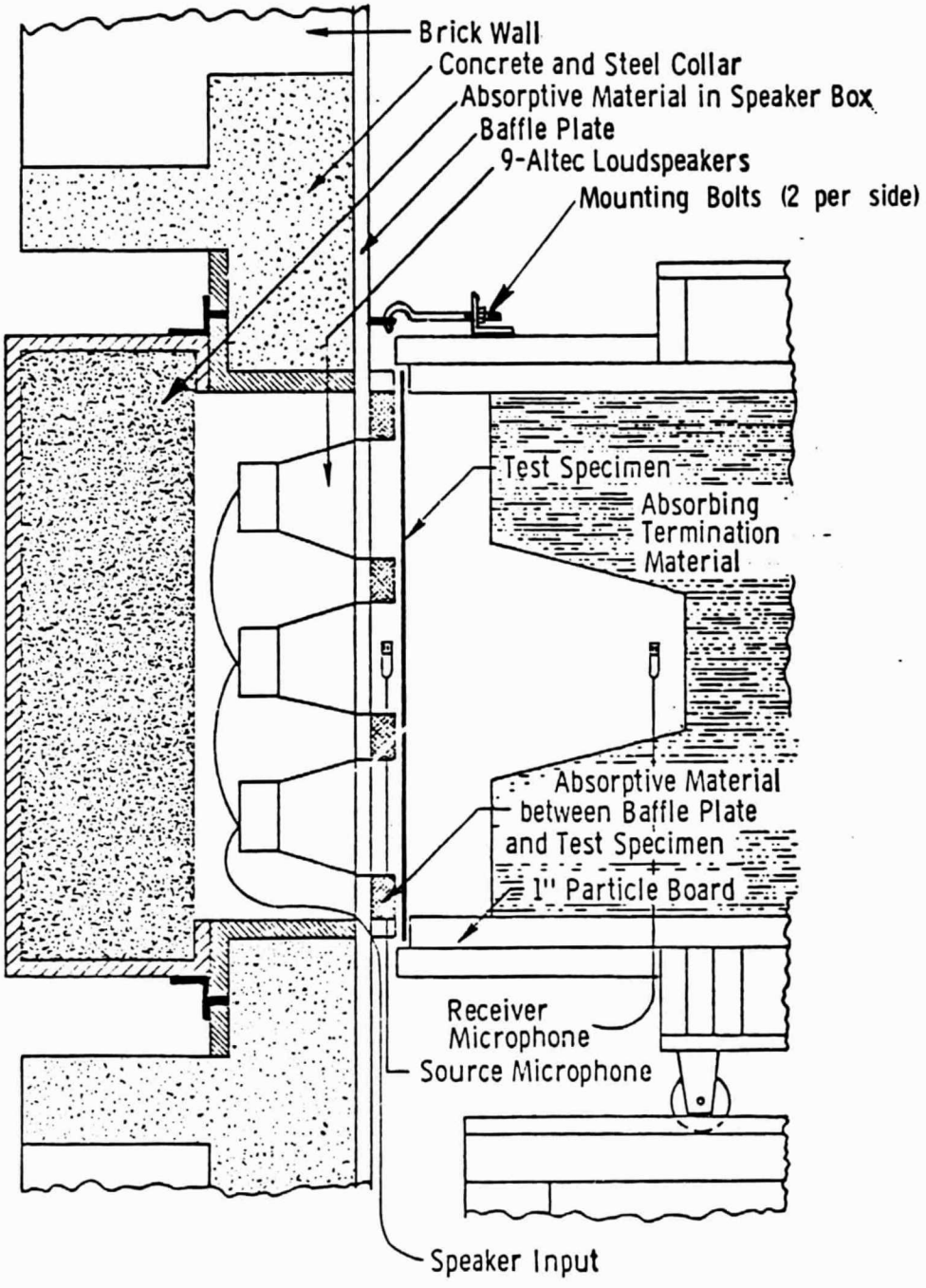

Figure 3.2: Panel Installation in the Beranek Tube

widest signal available on the oscillograph (approximately 3 inches, but this varies with frequency). The paper was then switched off to obtain a record of the signal decay. The paper speed was then adjusted to give a decay of about 3 inches for more accurate analysis and the test repeated until three good decays were obtained. Good is defined here as allowing the recorder enough time to speed up before switching the signal off and allowing the signal to decay fully before switching the recorder off. After the 3 good decays were recorded, the next peak (one which is not closely coupled or overshadowed by another peak) was located; and the preceding steps were repeated for each subsequent peak up to 1000 Hz.

3.5.2 Free Panel Tests

Several tests were performed on panels hung by a wire in front of the speakers, as shown in Figure 3.3, to minimize the effects of support-related damping (see Reference 27). These tests were used to check the validity of this decay test set-up by comparing the results for the free panel with those obtained by other investigators and for comparison with the panel installed in the tube to determine the support-related damping. The test procedure remained unchanged except that the accelerometer was mounted on a diagonal, since the middle of the panel is the intersection of two nodal lines for the first and several other modes, as shown in Figure 3.4. The cable from the accelerometer was routed to the nearest nodal line and off the panel at the intersection of the nodal line with the edge of the panel. Difficulties arose here at low frequencies be-

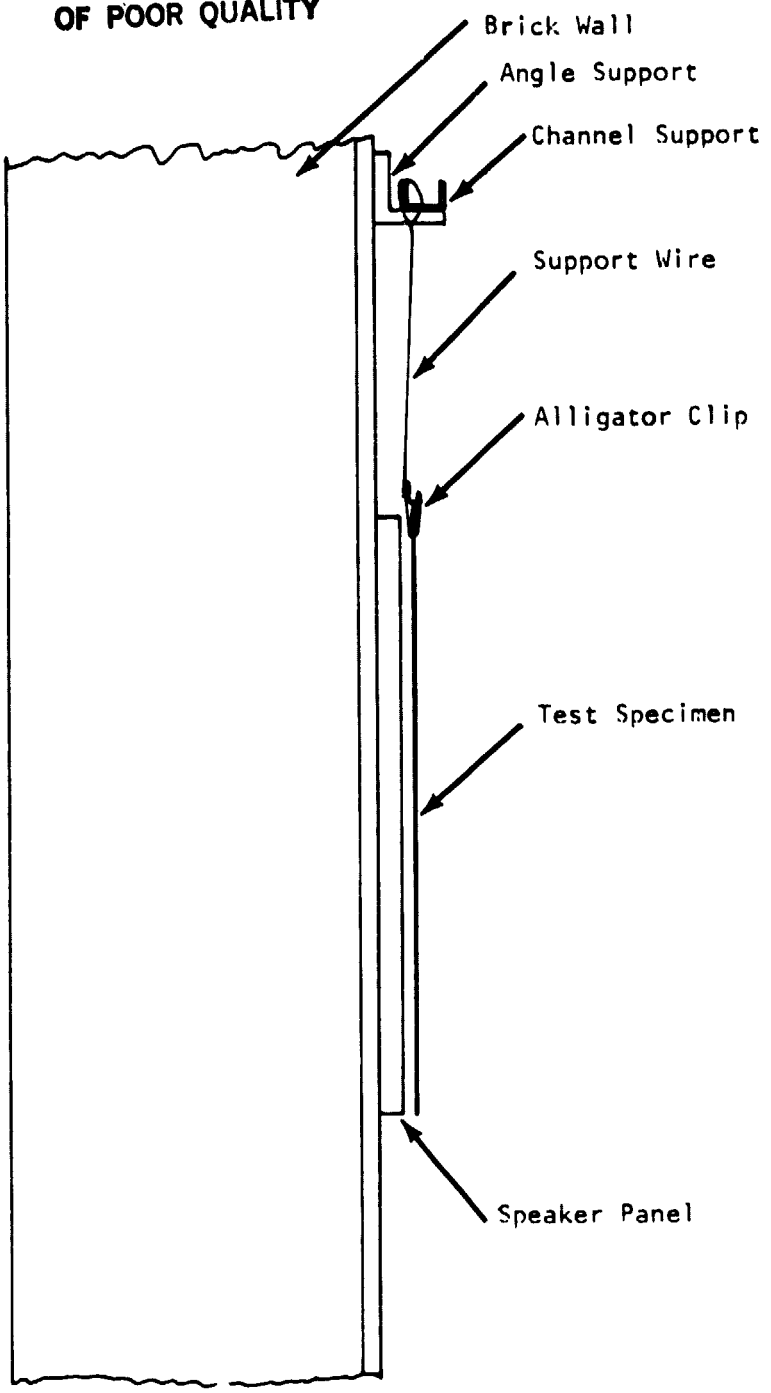

Figure 3.3: Hanging Panel Installation for the Free-free Modes (Side View)

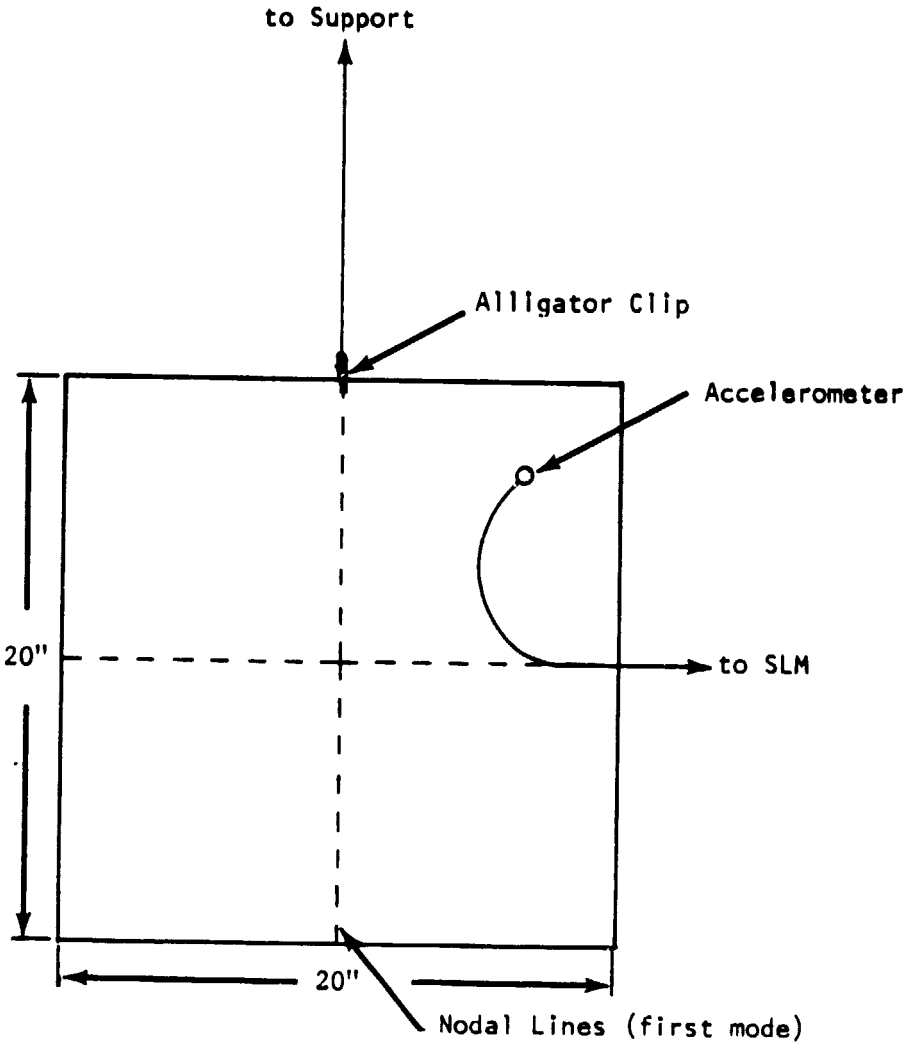

Figure 3.4: Front View of Hanging Panel Installation

cause the fundamental resonance frequency for the free panels was generally <10 Hz, which is far below the frequency range of the speaker set-up.

3.5.3 Special Considerations

a. Mass Effect of Accelerometer: The effect of the accelerometer mass on the panel natural frequency was checked using natural frequency relations for a beam with both ends supported and a central mass. These relations from Table 8-13 of Reference 9 for edge conditions between clamped and simply supported yielded a 0.7% decrease in the natural frequency due to the accelerometer, for an accelerometer mass of 2.7 gm and the mass of the lightest panel at 298 gm. This is certainly a negligible change. The cable and tape will similarly have an even small effect due to their mass and also should not affect the stiffness much if any.

b. Effect of a Closed Cavity: By placing the panel in a closed cavity, the effect of the pressure within the cavity could be significant, especially in the small space between the panel and the speakers. This effect was checked by recording the microphone signal simultaneously with the accelerometer signal. The results of these tests showed that for some modes there was a significant effect. That is, for the worst case noted the microphone signal decay rate was only 2 times faster than the panel decay rate. For a viable damping test,

the decay of the noise source should be an order of magnitude greater than the decay of the panel. The case presented here certainly violates this rule, but this was the worst case. For most panels, the microphone signal decay rate was significantly greater. Another factor entering here is that of acoustic damping of the panel. The effects of this damping were not examined here but should be in future studies.

3.6 DATA ANALAYSIS

To obtain the loss factor, η, from the decay curves, a workable relation was first obtained as follows.

$$\delta = 1/n \ln(x_0/x_n) \tag{3.6}$$

δ = the logaithmic decrement

x_0 = the amplitude of the damped wave at point 0

x_n = the amplitude of the damped wave after n cycles

n = the number of cycles.

For consistent results Plunkett (Reference 4) suggested counting the number of cycles, n_e, for the amplitude to decay to x_0/e.

$$\delta = 1/n_e \ln(e) \tag{3.7}$$

or

$$\delta = 1/n_e \tag{3.7a}$$

but

$$n_e = f*t_e \tag{3.8}$$

f = the frequency of vibration

t_e = the time to decay to x_0/e

and $$t_e = d_e/p.s. \qquad (3.9)$$

d_e = the distance to decay to x_0/e

p.s. = the recording paper speed

with the result that

$$\delta = p.s./(f*d_e) \qquad (3.10)$$

or in terms of

$$\eta = p.s./(\pi*f*d_e). \qquad (3.11)$$

3.6.1 Mechanical Curve Fit

The following procedure was then used to measure d_e from the decay curve.

1) Using a French curve (logarithmic) fair in a curve to fit the overall decay,
2) locate the first good peak and measure its height: This is x.
3) Divide x_0 by the numerical value of e.
4) On the decaying curve find where the value of x is equal to the result of step 3): This is point e.
5) Measure the distance between point 0 and point e: This is d_e.

A problem noted with the above procedure was that variation of the loss coefficient occurred depending on what part of the curve was fitted. This was only a problem with curves which deviated fairly significantly from the logarithmic decay, such as when mode interaction was evident or when Coulomb type damping was present. The variation introduced here was minimized by fitting the overall curve rather than a minor portion of it.

3.6.2 Linear Regression Curve Fit

This method involves digitizing the peaks of the decay curve and fitting a curve through the points. Both a linear and a logarithmic curve were fitted using linear regression for both. The correlation coefficient for each curve is used as a measure of the quality of the fit to indicate whether the damping is primarily Coulomb (indicated by a good linear fit) or viscous (indicated by a good logarithmic fit).

3.6.3 Comparison

A comparison of the two data analysis methods would be useful to see the positive or negative aspects or inconsistencies of each method. Three tests of a 0.032 inch thick aluminum panel were anlyzed by both methods. The results for the second method (computer) are consistently higher (by 8.7%) than those from the first method, but the overall trends for each method are nearly identical. The regression curve fit method would be expected to be more accurate than the mechanical curve fit. But as shown, either method will predict the overall trends of damping with the frequency; and results from the first method can be corrected to match those of the second method. One consideration is that the second method takes up to twice as long to obtain the results.

3.7 RESULTS

To check the validity of this test set-up and panel installation, several tests were run with panels of various materials and configura-

tions. Panels mounted to vibrate in the free-free modes were used to check the basic test set-up and for comparison with the installed panels to see what effect this installation has on the damping of the panels. Various clamping bolt torques were checked to approximate simply supported and clamped boundaries, and a heavy steel frame was used for a closer approximation of the clamped condition. The trends of damping variation with stress and frequency were measured and compared with results of other investigators. The effects of various stiffened, riveted, and bonded panel configurations were checked for comparison and for a closer approximation of actual aircraft boundary conditions. Finally, the effect of damping materials and composite material panels was measured. A list of the tests is given in Table 3.1.

3.7.1 Free Panel

The results from the free hanging panel tests on the bare aluminum panels of thickness 0.020 to 0.032 inches show that the loss factor at the lowest obtainable frequency was 0.002 to 0.004. This compares rather well with the loss factors from Heckl (Reference 10) for a free hanging bare panel of 0.0022. Large variations occurred for some frequencies. These were likely caused by the panel vibrating in a mode which caused the clip to vibrate, thus dissipating more energy and resulting in an increase in the measured damping.

Table 3.1: Damping Test Log

Test #	Test Description
1	0.020 Al, Free Panel
2	0.020 Al, Free, Stress effect
3	0.020 Al, Free
4	0.032 Al, Free
5	0.025 Al, Free, Active and 1/3 octave filter
6	0.032 Al, Free, 100% Y-370
7	0.025 Al, Stiffened (Channel & Z), Free
8	0.016 Al, 15"x15", Bonded
9	0.016 Al, 15"x15", Bolted edge strip
10	0.020 Al, 15"x15", Bonded
11	0.020 Al, 15"x15", Riveted
12	0.020 Al, new recorder set-up
13	0.025 Al, Standard
14	0.032 Al, Standard
15	0.032 Al, Effect of foam contact
16	0.032 Al, Test w/o foam over speakers
17	0.032 Al, 2 in. wide clamping frame
18	0.025 Al, Stiffened (Channel & Z) crossed
19	0.032 Al, 100% Y-370
20	2x0.016 Al, Bonded with IC-998
21	0-0-0, Graphite/epoxy
22	45-0-45, Graphite/epoxy
23	0.032 Al, Standard
24	0.032 Al, Standard
25	0.032 Al, Standard
26	$45\text{-}0^{u}\text{-}45$, Graphite/epoxy
27	0-45-0, Graphite/epoxy
28	0-0-0, Kevlar/epoxy
29	45-0-45, Kevlar/epoxy
30	0-45-0, Kevlar/epoxy

3.7.2 Installed Panel

To show the effect of the boundary conditions in the tube on the damping, a plot of the damping results for a 0.032 inch panel is shown in Figure 3.5 for both types of mounting. In addition, a plot for a 0.032 inch panel with a 2 inch wide by 0.25 inch thick steel clamping frame is shown. The figure shows that the installation has increased the damping of the panel by more than an order of magnitude. This same effect was also observed with the 0.020 and 0.025 inch thick aluminum panels. Comparison of the loss factors for the installed panel and the clamped panel shows that at the first two modes the frequencies and loss factors are in fair agreement. However, above this the installed panel damping is higher than for the clamped panel; and the frequencies are altered. This indicates that the boundary conditions for the installed panel approximate clamped for the lower modes but not at higher frequencies. Further tests should be done to check how well these boundaries approximate simply supported conditions. The loss factors for the clamped panel approach those for the free panel, as they should for the ideal case of no dissipation at the boundaries.

a. Repeatability of Runs: The consistency of the test method and the data reduction method can be checked by calculating the standard deviation in the results for several successive runs at each frequency. This was done for tests #23 and #24 with the 0.032 inch panel, with results shown in Table 3.2. The results of 4.9% and 3.7% for the average percentage standard deviation indicate that the loss factor for a given installation is within 5% of that measured.

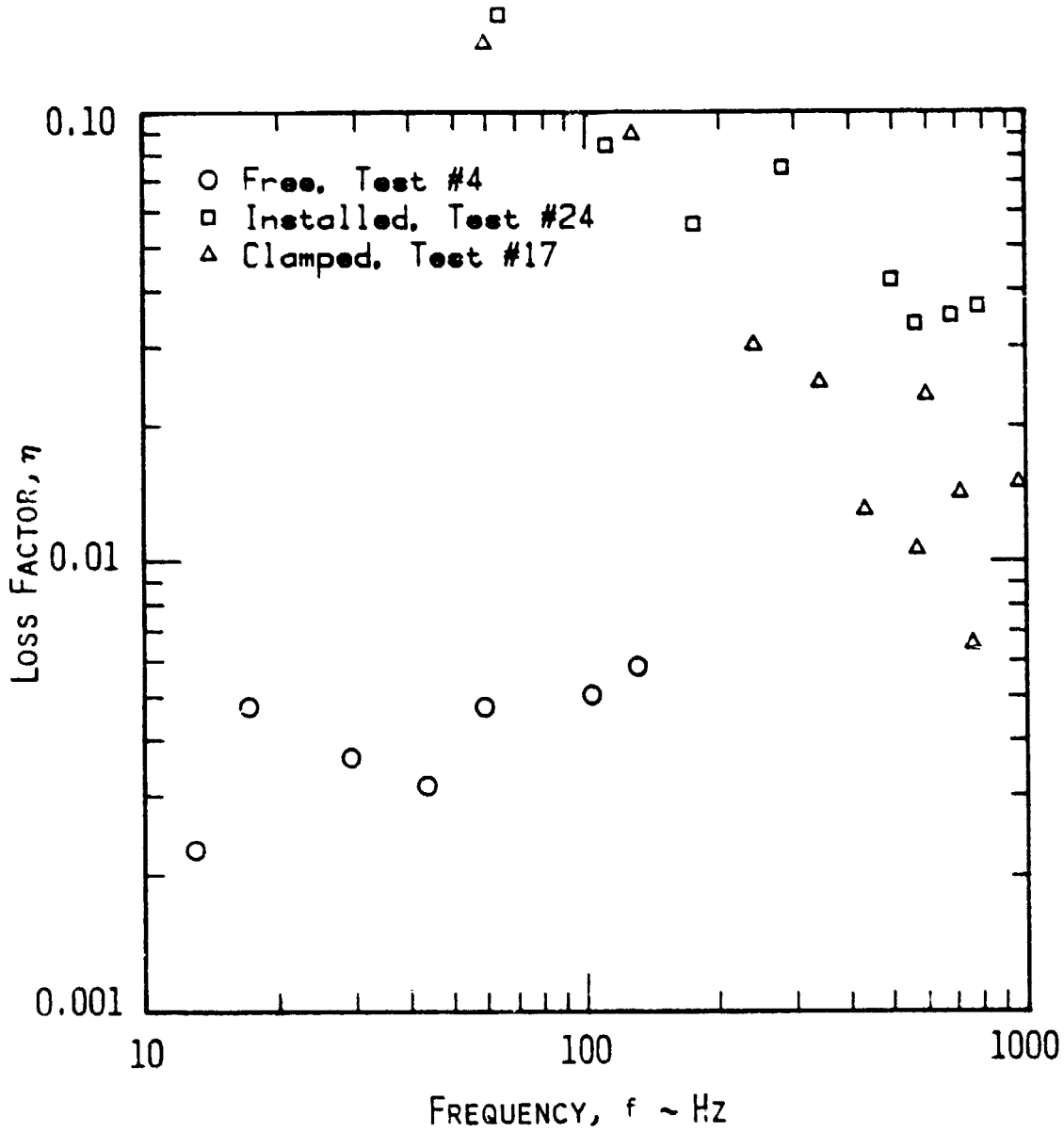

Figure 3.5: Effects of Boundary Conditions for a 0.032 Inch Aluminum Panel

Table 3.2: Percentage Standard Deviation for Tests #23 and #24

Test #23		Test #24	
f	$\sigma/\bar{x}$ (%)	f	$\sigma/\bar{x}$ (%)
116	0.1	112	4.9
178	1.4	177	3.7
289	5.8	281	6.0
502	15.1	498	5.1
572	5.8	564	1.5
689	4.6	680	2.2
792	1.6	785	2.1
Average	4.9%		3.7%

b. Clamping Torque: The effect of the clamping bolt torque on the loss factor was measured for a 0.020 inch panel, with the results shown in Figure 3.6. This simulates a transition from simply supported at 20 in-lb to clamped at 50 in-lb and with the clamping frame. The change in loss factor is negligible, as it should be. The only factor affecting this is the decreased amplitude due to the increased clamping on the panel causing a decrease in air damping, but this is compensated by the increase in stiffness of the "compliant" boundaries.

c. Successive Installations: Three tests were run on a standard 0.032 inch panel on different days to check the variations introduced due to the panel mounting technique. The results are shown in Figure 3.7. For the frequencies of 100 to 500 Hz, the variations are very small; but for the first mode and at the higher frequencies (<500 Hz), the variations were fairly large. For the fundamental mode this

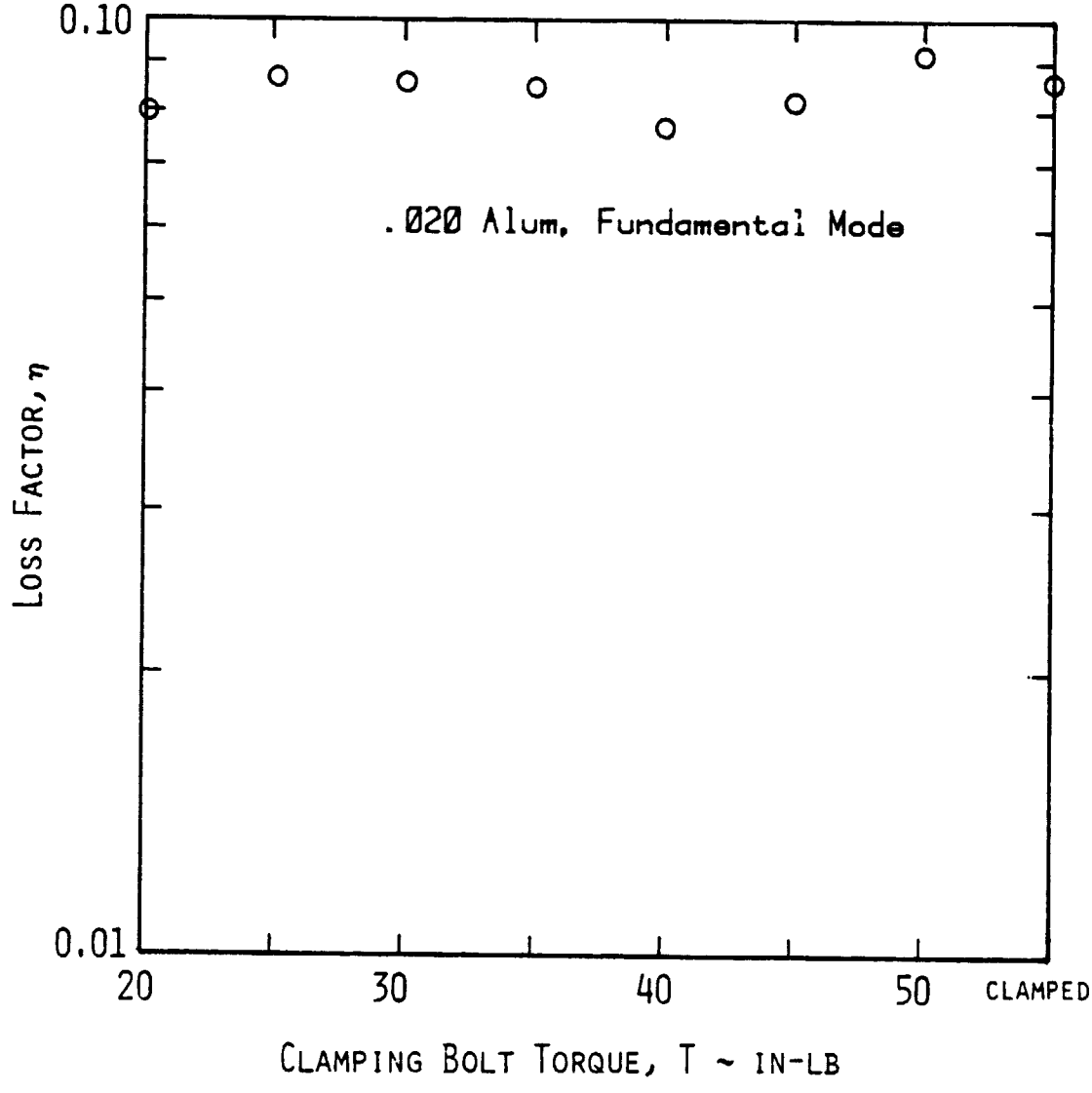

Figure 3.6: Effect of Clamping Bolt Torque on the Loss Factor for the Fundamental Mode of a 0.020 Inch Aluminum Panel

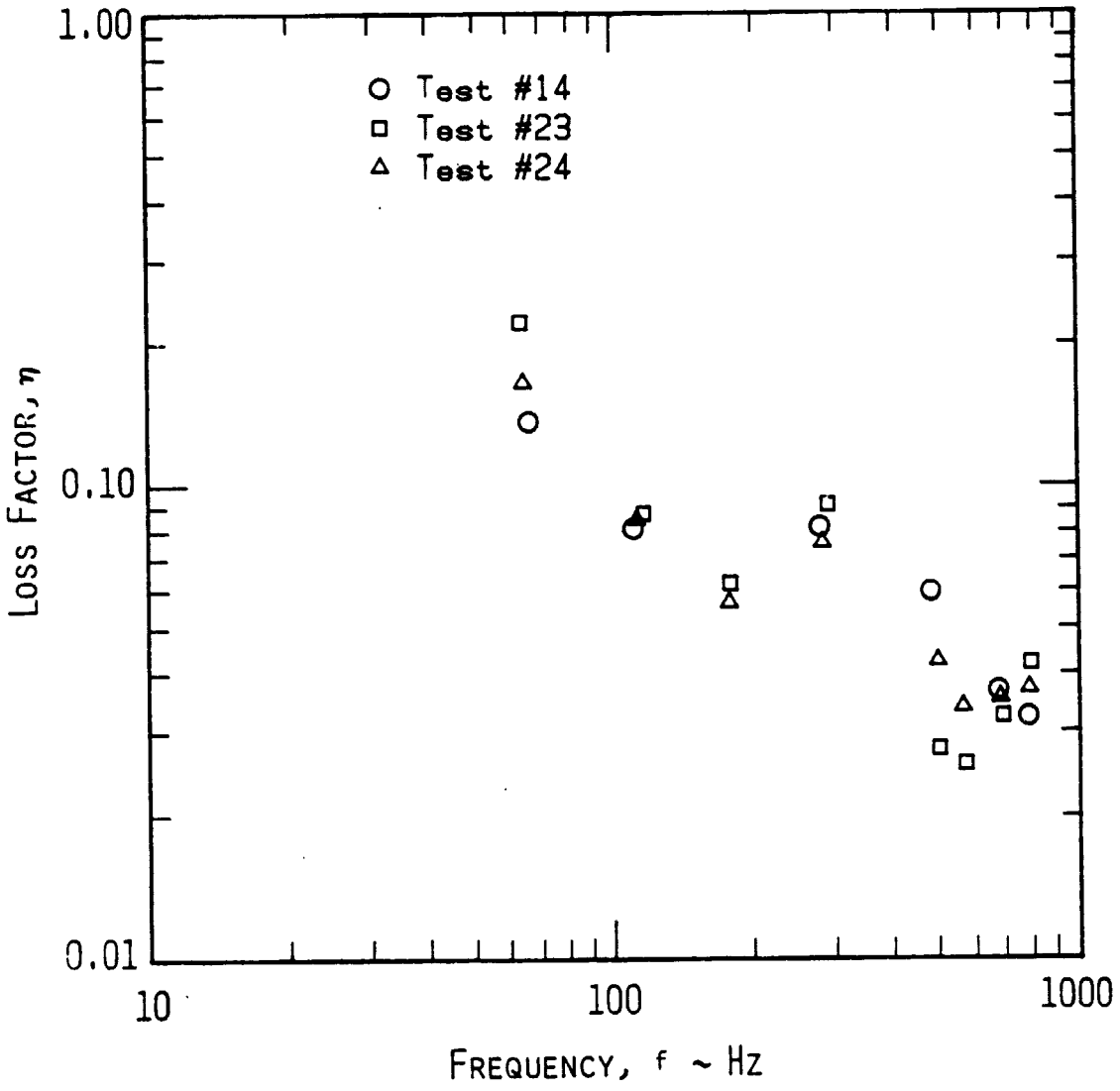

Figure 3.7: Comparison of Loss Factors for Successive Installations of a 0.032 Inch Aluminum Panel

variation can be attributed to the fact that the logarithmic curves did not fit the decay curves very well. The linear correlation factor was 0.99, while the logarithmic correlation factor was 0.95, indicating that the damping present was primarily Coulomb. At the higher frequencies this variation is possibly due to the alteration of the closely spaced higher modes upon each successive installation. Test #24 represents an average of the three, so this test will be used for comparison purposes in the following section.

3.7.3 Variation with Stress

a. Free: To check the effects of stress, one panel was excited at various sound pressure levels at a single frequency. The resulting loss factors are plotted as a function of the panel vibration amplitude (in terms of acceleration, since $a = \omega^2 x$ and ω is constant) in Figure 3.8. The trend is an increase in loss factor with the increase in amplitude. These results agree with the results of several investigators, including References 11 and 12. In addition, Granick and Stern (Reference 12) have shown that this trend is caused mainly by the air damping effect on the specimen (when operating at low stress levels). Crandall (Reference 13) shows the change in loss factor due to air damping for small amplitudes in a cantilever beam.

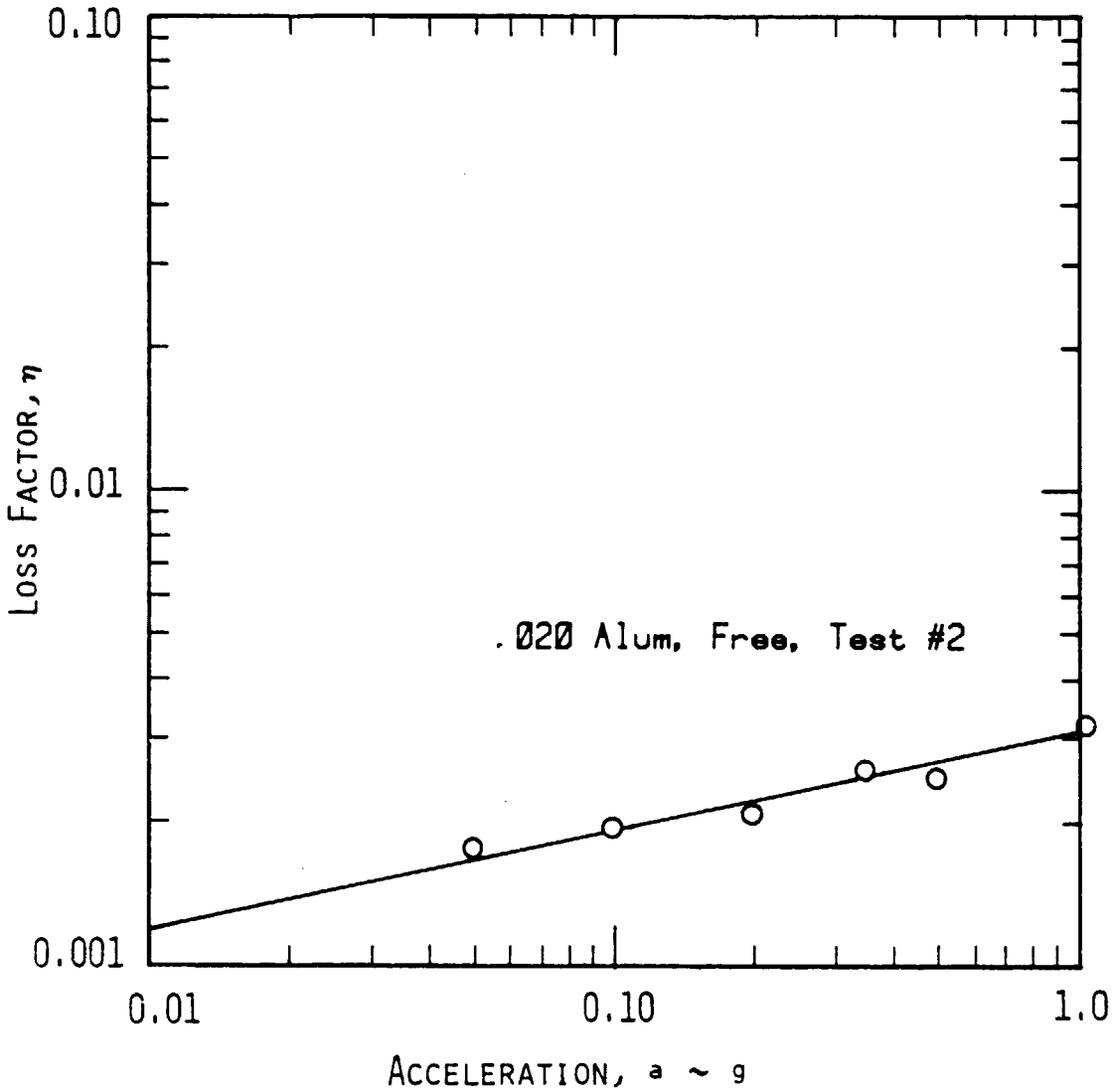

Figure 3.8: Effect of Acceleration (Displacement) on Damping for a 0.020 Inch Aluminum Panel for Free Boundaries

b. Installed: Similarly, a panel was placed in the Beranek tube and the loss factors calculated for a range of panel vibration amplitudes. The results shown in Figure 3.9 indicate a similar trend with a smaller slope (0.206 for the free panel, 0.129 for the installed panel). This difference could be caused by the difference in the mode shapes between the free and clamped panel. No references were found which investigated this effect.

3.7.4 Variation with Frequency

a. Free: Crandall (Reference 13) shows that aluminum is dependent on stress and frequency according to the relation

$$\eta\omega_1 = a^{(n/n + 1)} \tag{3.12}$$

where ω_1 is the frequency in rad/sec

a is the acceleration amplitude in g's

n is a material dependent constant.

The results for the aluminum panels were plotted based on this equation in Figure 3.10. The scatter of the data is fairly large, but the general trend is definitely present. This scatter could result from the fact that the loss factors were evaluated for various mode shapes rather than a single one as Crandall did. The value for n as obtained from the slope of the line is 4.2 rad/sec-g. This result is very high compared with Crandall's value of 0.77 and is probably due to the mode shape effects. A better test would be to

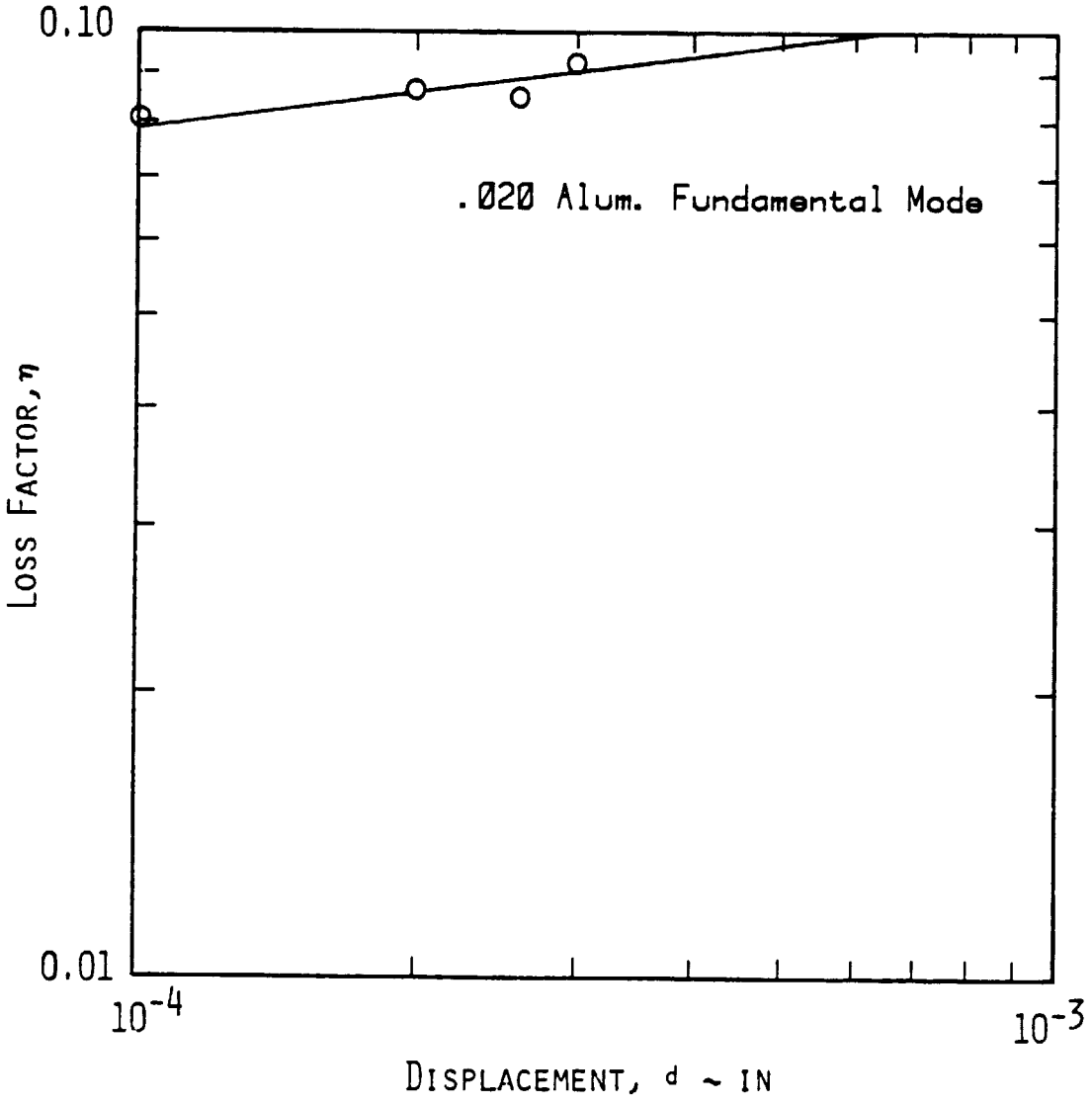

Figure 3.9: Effect of Displacement on Damping for the Fundamental Mode of a 0.020 Inch Aluminum Panel, Installed

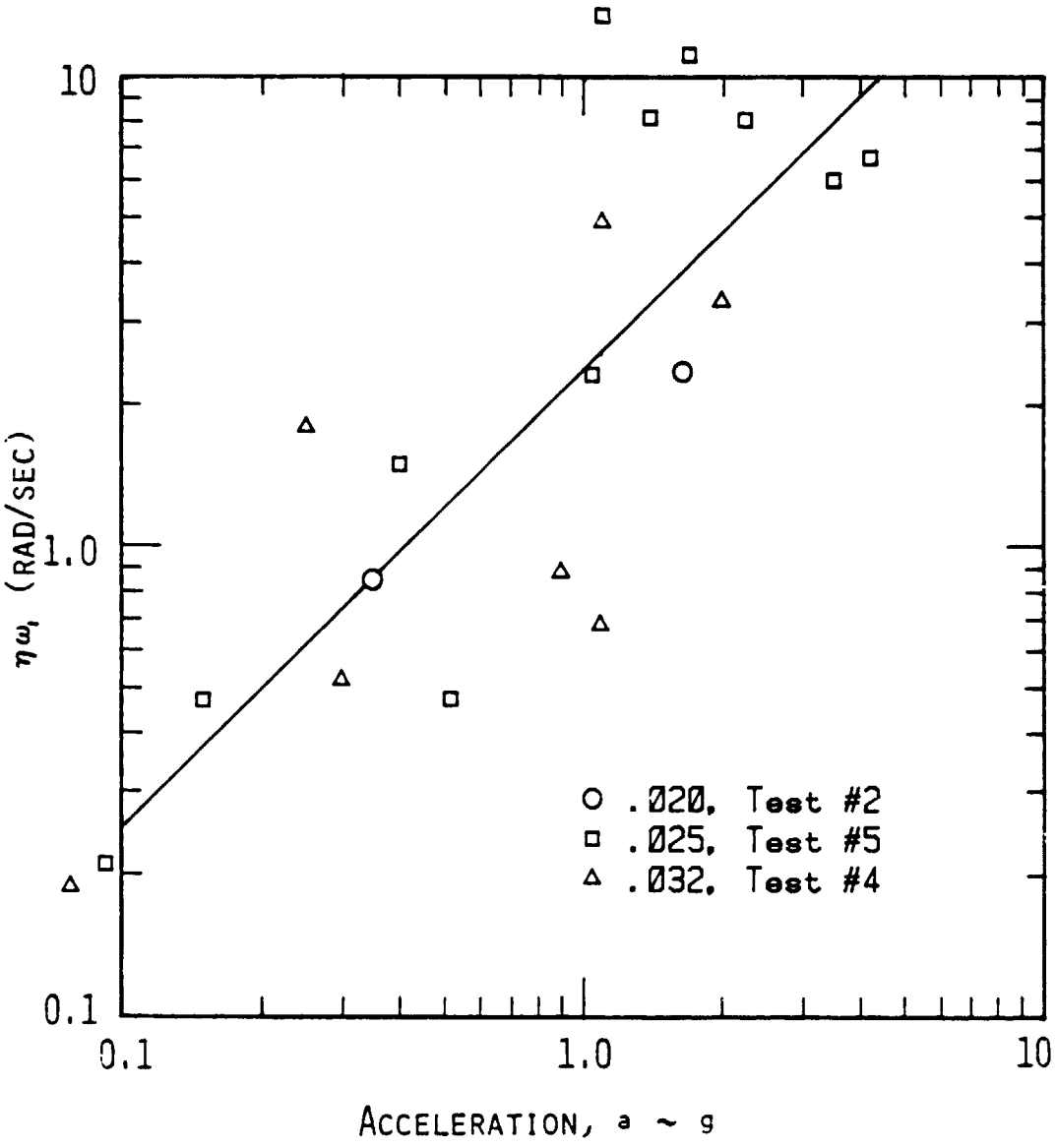

Figure 3.10: Attempt to Correlate Damping Data for Aluminum Panels According to Equation (3.12)

vary the size of the panel and thus its natural frequency and test the panel at its fundamental mode to eliminate the effect of the mode shapes.

b. Installed: Figure 3.7 shows the results for the 0.032 inch aluminum panel installed in the tube. This is typical of all the aluminum panels. The scatter of the data about a line fitted to the points may be contributed in part to the closed cavity effect mentioned in the previous chapter. Another effect here is that of modal damping, which varies with the frequency. Further study is suggested in this area to isolate these effects.

3.7.5 Effect of Stiffeners

To test the effect of stiffeners, a 0.025 inch aluminum panel with a channel stiffener and a "Z" stiffener crossed in the middle was tested, both free and mounted in the tube.

a. Free: A comparison of the loss factors for a stiffened plate with those of a bare plate as plotted in Figure 3.11 shows that at low frequencies there is no effect. At higher frequencies there is a noticeable increase in the damping. This increasing loss factor contribution with frequency agrees with the investigations by Ungar and Carbonell (Reference 14) and by Heckl (Reference 10), who show that this effect is caused by air pumping at the joints.

b. Installed: For the panels mounted in the tube, the results are shown in Figure 3.12. Here the effect of the stiffeners

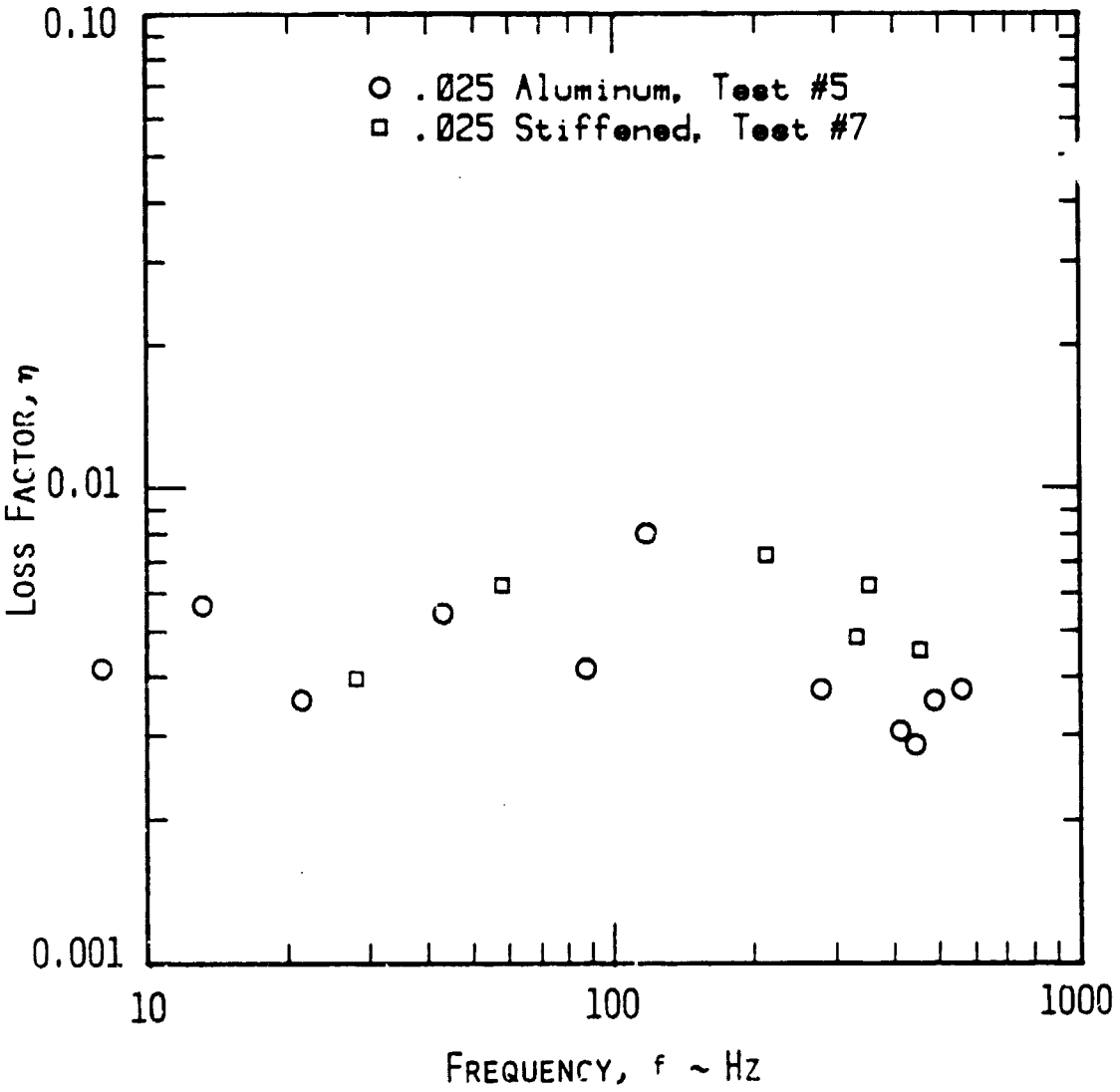

Figure 3.11: Effect of Stiffeners on Damping of a 0.025 Inch Aluminum Panel with Free Boundaries

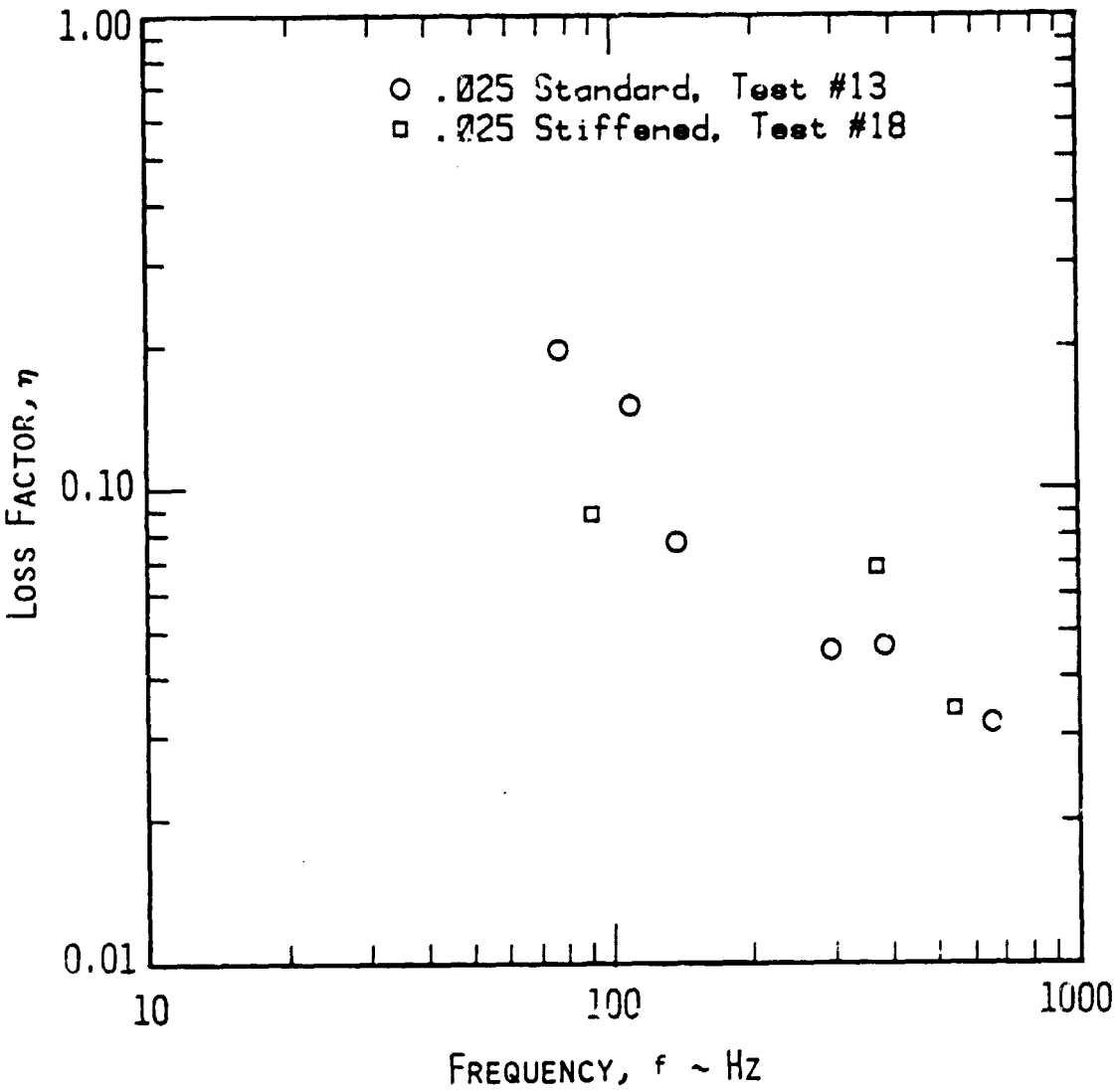

Figure 3.12: Effect of Stiffeners on Damping of a 0.025 Inch Aluminum Panel, Installed

is masked by the effect of the boundary conditions. Also, for the installed panels, the mode shapes of the stiffened panel were different than the bare panel due to the crossed stiffeners. For the free panels the mode shapes of the stiffened panel were the same as for the free panel.

3.7.6 Effect of Damping Material

For the evaluation of the testing of damping materials, two damped panels were tested. The first panel was a 20 x 20 x 0.032 inch aluminum panel with Y-370 damping material over an 18 x 18 inch area of the panel. The second panel consisted of a 20 x 20 x 0.016 inch aluminum panel with a 17.6 x 17.6 x 0.016 inch aluminum panel bonded to this with IC-998 viscoelastic adhesive. The first panel was tested for both free and installed mounting, while the second was tested only for the installed condition.

a. Free: As shown in Figure 3.13, the damping material had a definite effect on the loss factor with a $\Delta\eta$ of about 0.075. This increase by more than an order of magnitude corresponds well with the results of Crandall (Reference 32) for a free-free beam.

b. Installed: Figure 3.14 shows the results for the two damped panels mounted in the tube, comparing them with the results for the bare panel. The overall effect is seen to be an increase in damping at the higher frequencies and not much effect at the lowest frequency. The two materials seem to behave the same over the entire range. The

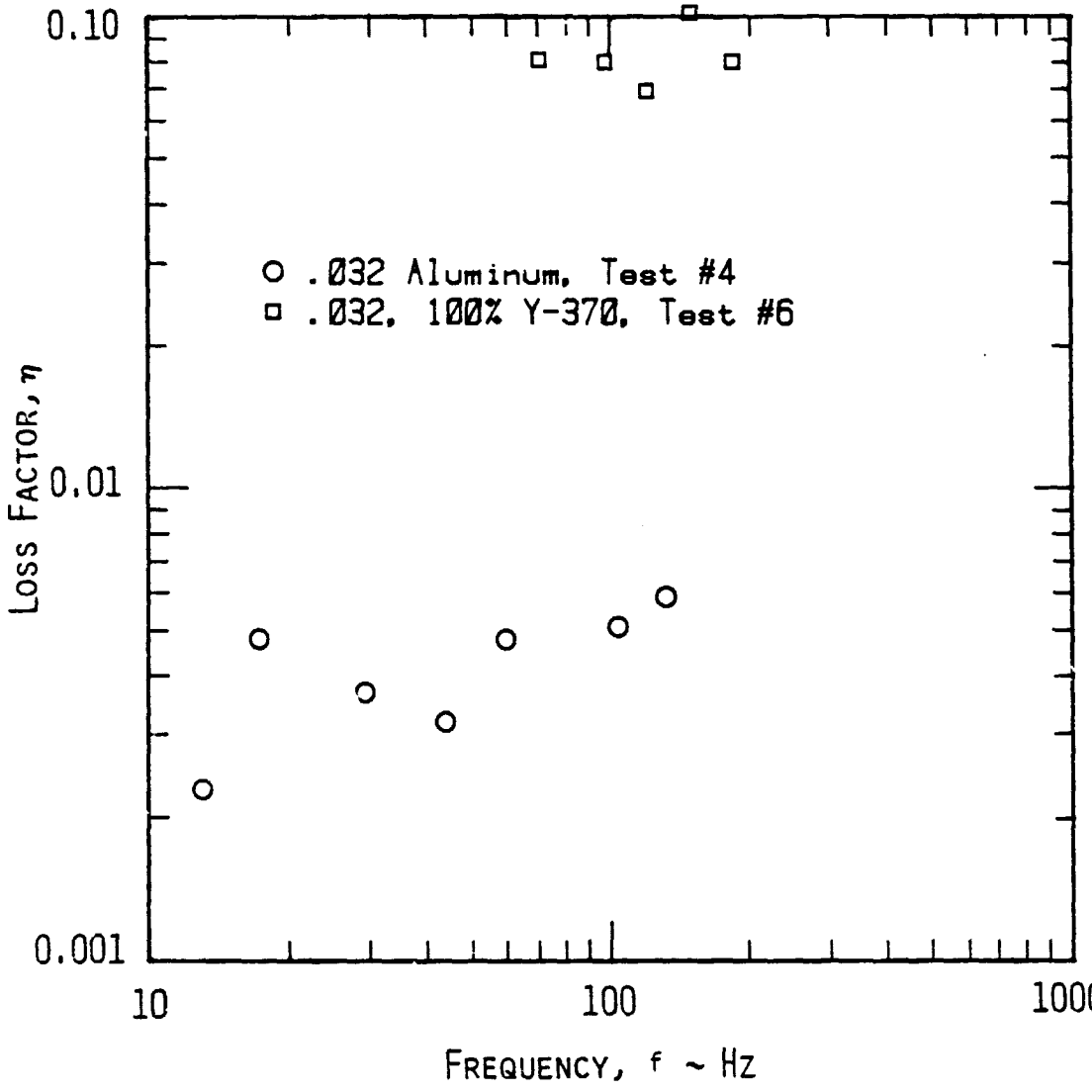

Figure 3.13: Effect of 100% Y-370 Damping Material on Damping of ε 0.032 Inch Aluminum Panel with Free Boundaries

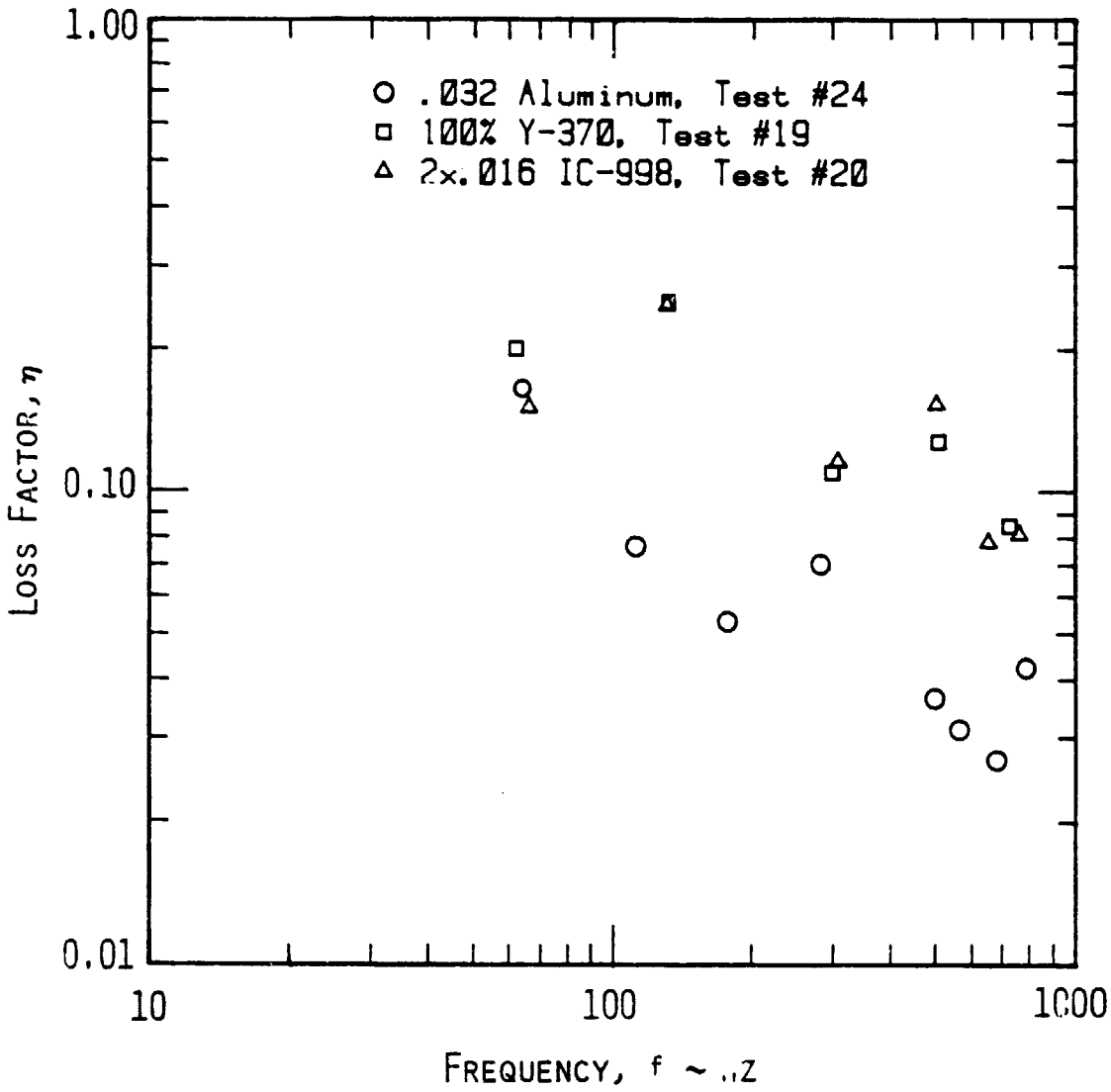

Figure 3.14: Effect of 100% Y-370 and Panels Bonded with IC-998 Adhesive on Damping of a 0.032 Inch Aluminum Panel, Installed

$\Delta\eta$ is about the same for the frequency range 500-1000 Hz as it was for the free panels.

3.7.7 Composite Panels

Graphite/epoxy and Kevlar/epoxy panels of various ply orientations were tested in the tube with loss factor results as shown in Figures 3.15 and 3.16. There are no particular ply orientations that stand out as having much better damping than the others for either the graphite or the Kevlar panels. The scatter for the Kevlar is larger than for the graphite composites, possibly due to manufacturing tolerances; but the average damping and the decrease with frequency are very close. These panels show approximately a 30% increase in damping ($\Delta\eta$ = .03) over the aluminum panel of comparable thichness (0.032) at the lowest frequency and none at the higher frequencies. Several investigators (References 41 through 44) have shown that, for certain ply orientations, the damping can be up to 20 times that of aluminum; but the effects here are partially masked by the boundary losses. The scatter in the data here is mainly due to the many factors which affect the damping of composite panels in addition to the previously mentioned effects of this installation on aluminum panels. One of these factors is the fiber volume fraction of the composite (References 45 and 46) which is unknown for these panels.

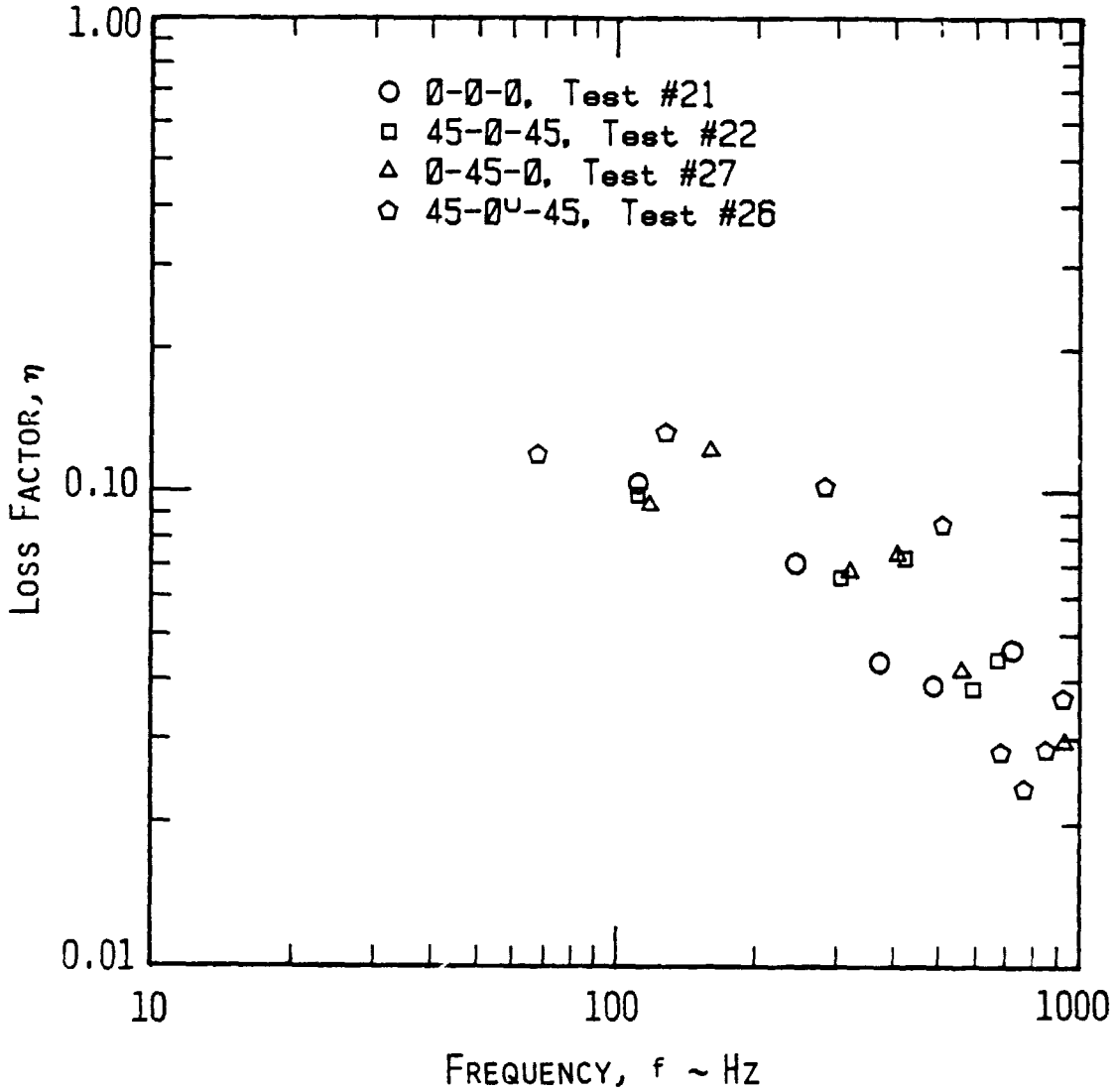

Figure 3.15: Damping in Graphite/Epoxy Panels of Various Ply Orientations, Installed

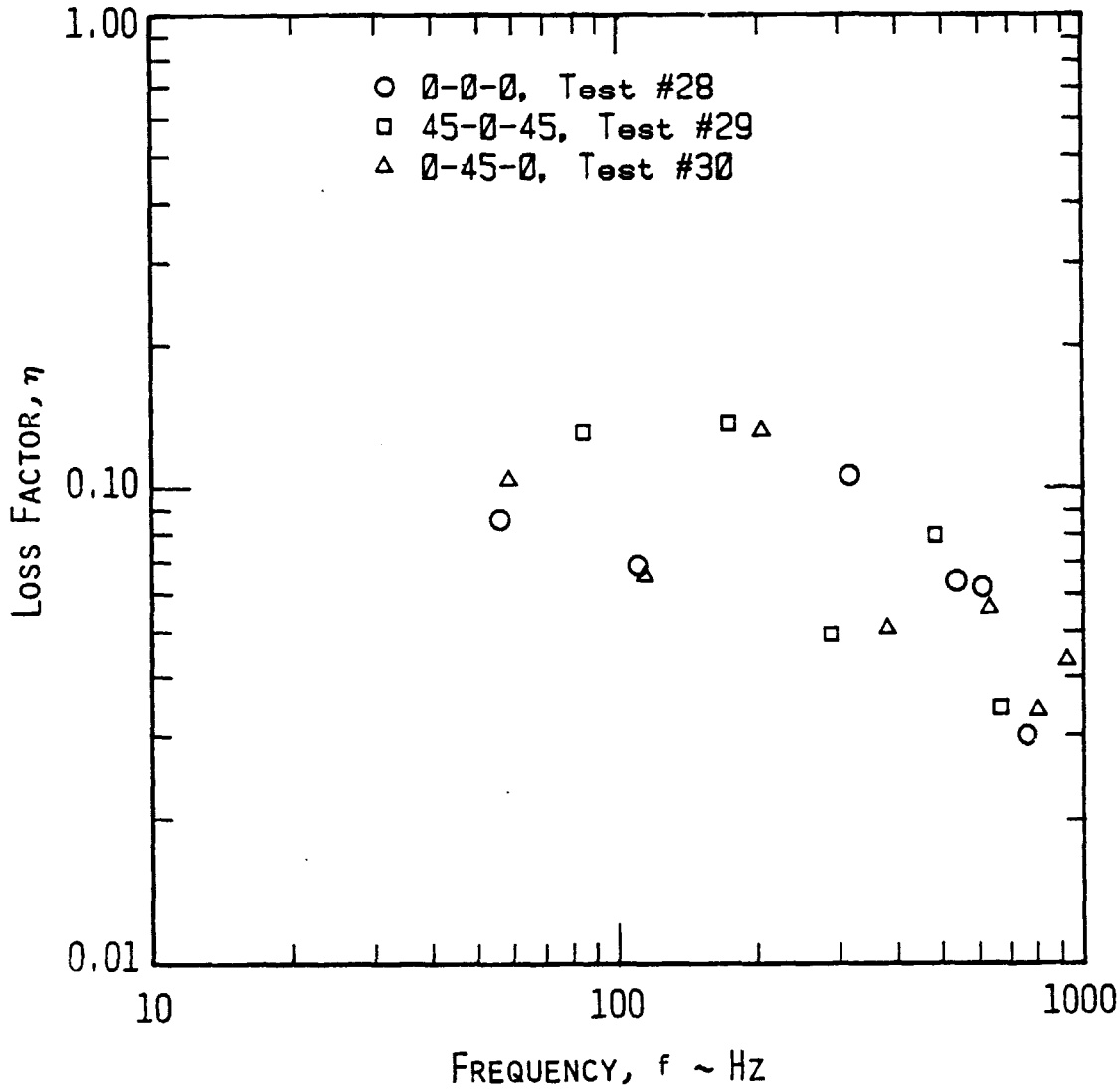

Figure 3.16: Damping in Kevlar/Epoxy Panels of Various Ply Orientations, Installed

3.7.8 Bonding and Riveting

To obtain edge conditions which approximate those typical of an aircraft structure, special panels were constructed. Panels measuring 12 x 12 inches were attached to aluminum strips by bonding or riveting. These aluminum strips were clamped to a special test device, described in Reference 47, by a one-inch-wide steel strap and screws.

A panel similar to the 20 x 20 inch panels tested was tested with the special test device for comparison with both the "realistic" edge conditions and to check the effect of the closed cavity. Figure 3.17 shows results for the clamped panel and a bonded panel. The clamped panel demonstrates a characteristics curve very close to that of the 0.032 inch panel with the clamping frame; thus, the effect of the closed cavity on the panel damping can be assumed to be negligible for this case. The bonded panel had higher damping and very linear characteristics. Figure 3.18 shows a comparison of the loss factors for a bonded and a riveted panel. The value for η of 0.024 agrees with the results obtained by Ballentine (Reference 48) for typical aircraft panels. The bonded panel has higher damping at the frequencies up to about 700 Hz, where it intersects the line corresponding to the riveted panel and the riveted panel begins to have higher damping than the bonded panel. This phenomenon is probably due to the effectiveness of the viscoelastic damping of the bonding material at low frequencies, while the damping of the riveted panel caused by air pumping and slip at the joints is more effective at higher frequencies (Reference 40). But there is an overall decrease

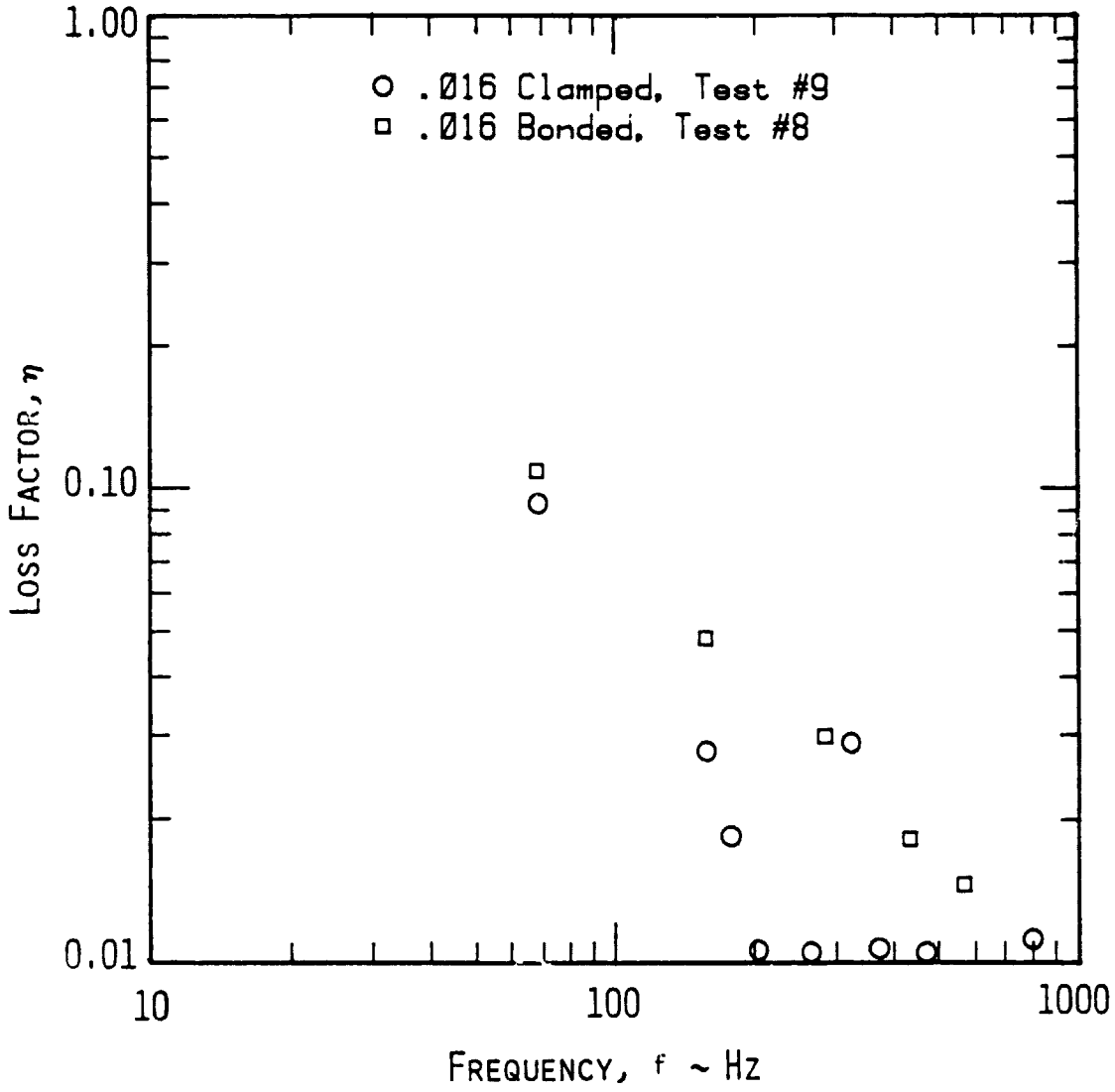

Figure 3.17: Effect of Bonded and Clamped Edge Conditions on Damping of 0.016 Inch Aluminum Panels Mounted in the Special Test Device

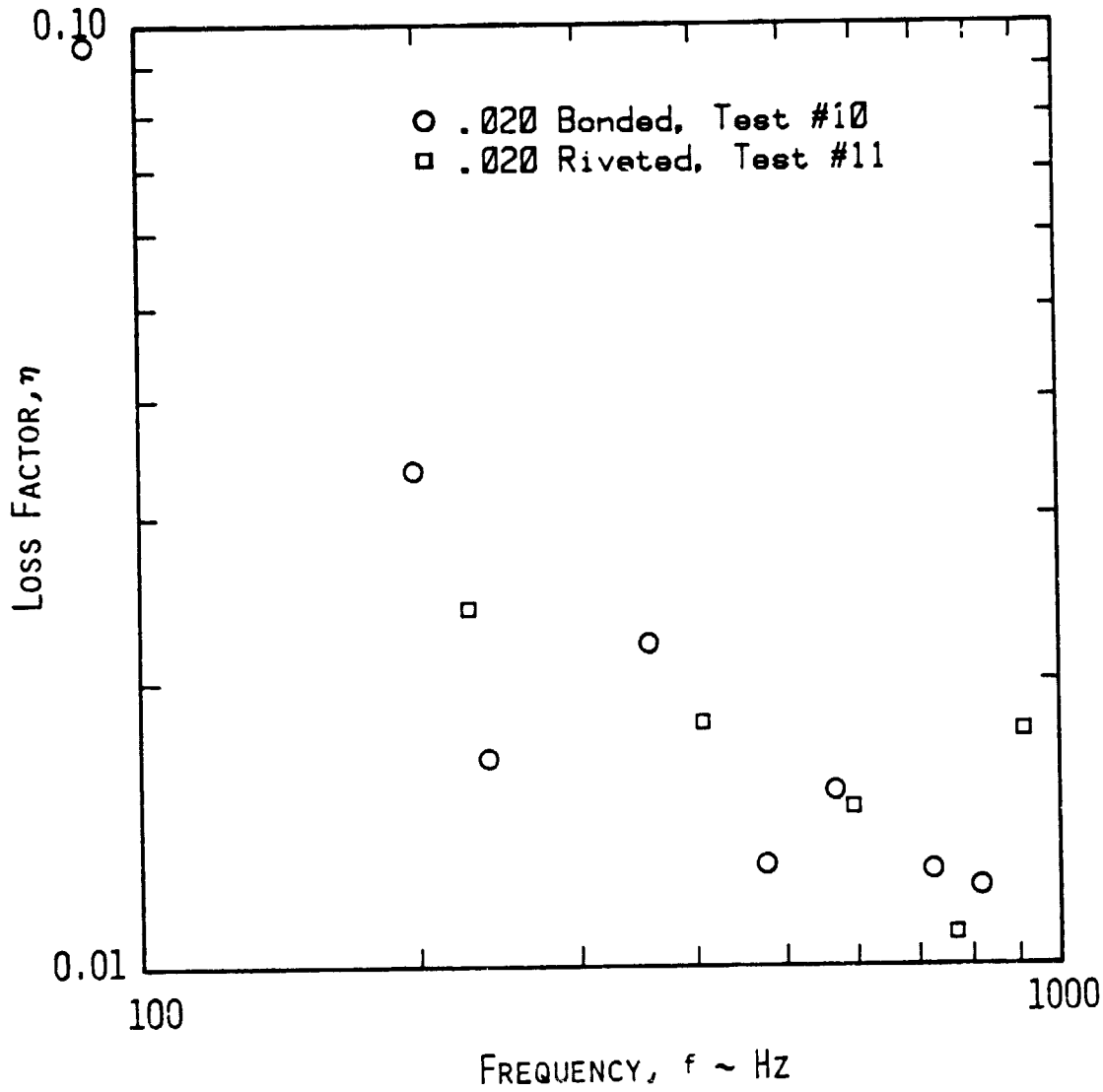

Figure 3.18: Effect of Bonded and Riveted Edge Conditions on Damping of 0.020 Inch Aluminum Panels Mounted in the Special Test Device

in damping because of the decreasing amplitude of the vibration, as shown by Mead (Reference 28).

3.8 CONCLUSIONS AND RECOMMENDATIONS

The decay rate tests worked very simply with the existing equipment and show what type of damping is present for each mode. The testing method used here produced results which were consistent within 5% for each installation, which is very good for this type of installation. Both methods of data analysis produced comparably consistent results over a wide frequency range, with a difference of less than 10% between the two.

Tests conducted on panels suspended by a wire at the nodal point verified the basic equipment set-up and test procedure and provided a comparison with the results for the installed panels, showing the contribution of the boundary conditions to the overall damping of the panel. The torque on the clamping bolts showed no effect on the damping. Variations in the experimental damping for successive installations were within 10% for lower frequencies but varied considerably for the higher frequencies. There was a 50% decrease in the effect of stress as a result of the panel installation.

The effects of the panel installation tend to mask the increased damping due to stiffeners, damping material, and composite materials; but their effects are still generally noticeable. The special installation used to test the panels with "realistic" edge conditions actually resulted in two checks. The riveted and bonded panels indeed have higher damping than the clamped panel; but relative to each other,

there is no advantage of one over the other. The by-product of this test was that the closed cavity effect on the damping proves to be negligible but does cause increased scatter of the data.

As a result of this series of checks, the damping test procedure as described here can be used to obtain loss factors accurate to within 10% for frequencies up to about 500 Hz. For the fundamental frequency and for higher frequencies, care must be taken when using these results. For general use, there loss factors can be obtained by averaging the results for several successive installations. When more specific results are required, it is suggested that the decay tests and the noise reduction tests be done successively without removing the panel. If stress effects are important in a certain analysis, these can be taken into account using the results for both a free and an installed panel. It is recommended that the effects of acoustic radiation on the panel damping be analyzed theoretically and/or experimentally. Also panels should be tested in a device which approximates a simply supported boundary to check how closely the regular panel installation approximates the simply supported boundaries.

REFERENCES

1. Laméris, J., Stevenson, S., Streeter, B., "Study of Noise Reduction Characteristics of Composite Fiber-Reinforced Panels, Interior Trim Panel Configurations, and the Application of the Tuned Damper Concept," KU-FRL-417-18, University of Kansas Flight Research Laboratory, Lawrence, Kansas, March 1982.
2. Roskam, J., Grosveld, F., and van Aken, J., "Summary of Noise Reduction Characteristics of Typical General Aviation Materials," KU-FRL-317-P6, SAE paper No. 790627, included in Transactions of the SAE, August 1980.
3. Grosveld, F., Navaneethan, R., "Noise Reduction Characteristics of Flat, General Aviation Type Pane Windows," KU-FRL-417-12, University of Kansas Flight Research Laboratory, Lawrence, Kansas, February 1980.
4. Grosveld, F., Laméris, J., "The Effect of Oblique Angle of Sound Incidence, Realistic Edge Conditions, Curvature, and In-Plane Panel Stresses on the Noise Reduction Characteristics of General Aviation Type Panels," KU-FRL-417-10, University of Kansas Flight Laboratory, Lawrence, Kansas, July 1979.
5. Navaneethan, R., "Study of Noise Reduction Characteristics of Multilayered Panels and Dual Pane Windows with Helmholtz Resonators," KU-FRL-417-16, University of Kansas Flight Research Laboratory, Lawrence, Kansas, May 1981.
6. Navaneethan, R., Streeter, B., Koontz, S., "Influence of Depressurization and Damping Material on the Noise Reduction Character-

istics of Flat and Curved Stiffened Panels," KU-FRL-417-17, University of Kansas Flight Research Laboratory, Lawrence, Kansas, October 1981.

7. Dowell, E. H., "Master Plan for Prediction of Vehicle Interior Noise," AIAA Journal, Vol. 18, No. 4, 1980.

8. Koval, L. R., "Effect of Airflow, Panel Curvature, and Internal Pressurization on Field Incidence Transmission Loss," J. Acoust. Soc. Am., Vol. 59, No. 6, June 1976.

9. Koval, L. R., "On Sound Transmission into a Thin Cylindrical Shell and Flight Conditions," J. S. & V., Volume 48 (2), pages 265-275, 1976.

10. Koval, L. R., "On Sound Transmission into a Stiffened Cylindrical Shell under Flight Conditions," presented at 3rd AIAA Aero Acoustics Conference, Palo Alto, California, July 20-23, 1976.

11. Koval, L. R., "Effect of Cavity Resonances on Sound Transmission into a Thin Cylindrical Shell," J. S. & V., Vol. 59 (1), pages 23-33, 1978.

12. Koval, L. R., "Effect of Longitudinal Stringers on Sound Transmission into a Thin Cylindrical Shell," J. Aircraft, Vol. 15, No. 12, December 1978.

13. Beranek, L. L., and Work, George A., "Sound Transmission through Multiple Structures Containing Flexible Blankets," J. Acoust. Soc. Am., Vol. 21, pages 419-428, 1949.

14. Cockburn, J. A., and Jolly, A. C., "Structural-Acoustic Response, Noise Transmission Losses and Interior Noise Levels of an Aircraft Fuselage Excited by Random Pressure Fields," AFFDL-TR-68-2, 1968.

15. Rennison, D. C., et al., "Interior Noise Control Prediction Study for High-Speed Propeller Driven Aircraft," NASA CR 159200, NASA September 1979.

16. Revell, J. D., Balina, F. J., and Koval, L. R., "Analytical Study of Interior Noise Control by Fuselage Design Techniques on High-Speed Propeller Driven Aircraft," NASA CR 159222, July 1978.

17. Dowell, E. H., Gorman, G. F. III, and Smith, D. A., "Acousto-elasticity: General Theory, Acoustic Natural Modes and Forced Response to Sinusoidal Excitation, Including Comparisons with Experiments," J. S. & V., Volume 52 (4), pages 519-542, 1977.

18. Dowell, E. H., "Turbo Prop Interior Noise Studies," presented at AIAA 5th Aero Acoustics Conference, Seattle, Washington, March 12-14, 1979.

19. Vacaitis, R., "Noise Transmission into a Light Aircraft," J. Aircraft, Vol. 17, No. 2, February 1980.

20. Vacaitis, R., Slazak, M., and Chany, M. T., "Noise Transmission Turbo Prop Problem," AIAA 5th Aero Acoustics Conference, Seattle, Washington, March 12-14, 1979.

21. Miller, V. R., Faulkner, L. L., "Prediction of Aircraft Interior Noise Using the Statistical Energy Analysis Method," 81-DET-102 ASME, presented at the Design Engineering Technical Conference, September 20-23, 1981, Hartford, Connecticut.

22. Pope, L. D., and Wilby, J. F., "Band Limited Power Flow into Enclosures," J. Acoust. Soc. Am., Vol. 62, No. 4, October 1977.

23. Pope, L. D., and Wilby, J. F., "Band-Limited Power Flow into Enclosures II," J. Accust. Soc. Am., Vol. 67, No. 3, March 1980.

24. Wilby, J. F., and Pope, L. D., "Prediction of the Acoustic Environment in the Space Shuttle Payload Bay," AIAA 5th Aero Acoustics Conference, Seattle, Washington, March 12-14, 1979.

25. Pope, L. D., Rennison, D. C., and Wilby, E. G., "Analytical Prediction of the Interior Noise for Cylindrical Models of Aircraft Fuselages for Prescribed Exterior Noise Fields: Phase I," NASA CR 159363, October 1980.

26. Barton, C. K., "Structural Stiffening as an Interior Noise Control Technique for Light Twin Engine Aircraft," PhD Thesis, N.C. State University, Raleigh, N.C., 1979.

27. Beranek, L. L., Noise and Vibration Control, McGraw-Hill Publications, New York, 1971.

28. Mead, Danys J., "Prediction of the Structural Damping of a Vibrating Stiffened Plate," Damping Effects in Aerospace Structures, AGARD CP 277, pages 2-1 through 2-15.

29. Paz, Mario, Structural Dynamics, VanNostrand Reinhold Company, 1980.

30. Plunkett, R., "Measurement of Damping," Section Five, Structural Damping, Ed. by Jerome E. Ruzicka, The American Society of Mechanical Engineers, Shock and Vibration Committee, pages 117-131, 1959.

31. Bert, C. W., "Material Damping: An Introductory Review of Mathematical Models, Measures and Experimental Techniques," J. S. & V., Vol. 29 (2), pages 129-153, 1973.

32. Crandall, Stephen H., "On Scaling Laws for Material Damping," NASA TN D-1467.

33. Lazan, B. J., Damping of Materials and Members in Structural Mechanics, Pergamon Press, Inc., 1968.

34. Bruel & Kjaer, Piezoelectric Accelerometer and Vibration Preamplifier Handbook, Rev. March 1978.

35. Blevins, Robert D., Formulas for Natural Frequency and Mode Shape, Van Nostrand Reinhold Company, 1979.

36. Heckl, Manfred, "Measurements of Absorption Coefficients on Plates," J. Acoust. Soc. Am., Vol. 34, No. 6, June 1962, pages 803-808.

37. Lee, J. M., and McConnell, K. G., "Experimental Cross Verification of Damping in Three Metals," Experimental Mechanics, Vol, 42, September 1975, pages 347-353.

38. Granick, Neal, and Stern, Jesse, "Material Damping of Aluminum by a Resonant-Dwell Technique," NASA TN D-2893.

39. Crandall, S. H., "The Role of Damping in Vibration Theory," J. S. and V., Vol. 11, No. 1, 1970, pages 3-18.

40. Ungar, E. E., and Carbonell, J. R., "On Panel Vibration Damping Due to Structural Joints," AIAA Journal, Vol. 4, No. 8, August 1966, pages 1385-1390.

41. Mazza, L. T., Paxson, E. B., and Rodgers, R. L., "Measurement of Damping Coefficients and Dynamic Modulus of Fiber Composites," USAAVLABS Technical Note 2, U.S. Army Aviation Materiel Laboratories, Fort Eustis, Virginia, February 1970.

42. Adams, R. D., and Bacon, D. G. C., "Effects of Fiber Orientation and Laminate Geometry on the Dynamic Properties of CFRP," J. of Composite Materials, Vol. 7, October 1973, pages 402-428.

43. Schultz, Albert B., and Tsai, Stephen W., "Dynamic Moduli and Damping Ratios in Fiber-Reinforced Composites," J. of Composite Materials, Vol. 2, No. 3, July 1968, pages 368-379.

44. Schultz, Albert B., and Tsai, Stephen W., "Measurements of Complex Dynamic Moduli for Laminated Fiber-Reinforced Composites," J. of Composite Materials, Vol. 3, July 1969, pages 434-443.

45. Adams, Robert D., and Bacon, D. G. C., "The Dynamic Properties of Unidirectional Fibre Reinforced Composites in Flexure and Torsion," J. of Composite Materials, Vol. 7, January 1973, pages 53-66.

46. Adams, et al., "Three Dynamic Properties of Unidirectional Carbon and Glass Fiber Reinforced Plastics in Torsion and Flexure," J. of Composite Materials, Vol. 3, October 1969. pages 594-603.

47. Grosveld, Ferd, et al., "The Effect of Oblique Angle of Sound Incidence, Realistic Edge Conditions, Curvature and In-Plane Panel Stresses on the Noise Reduction Characteristics of General Aviation Type Panels," KU-FRL-417-10, Progress Report for NASA Grant NSG 1301, University of Kansas, Lawrence, Kansas, July 1979.

48. Ballentine, J., et al., "Refinement of Sonic Fatigue Structural Design Criteria," AFFDL-TF-67-156, January 1968.

49. Anon., "Strain Gage Installations with M-Bond 200 Adhesive," Micro-Measurements Instruction Bulletin B-127-5, May 1976.

APPENDIX A

EQUATIONS USED IN INTERIOR NOISE CONTROL PROGRAM

A.1 THE EQUATIONS USED IN THE MODEL

The computer program at the KU-FRL closely follows that developed in References 15 and 16. The noise reduction across a panel is given by

$$NR = 10 \text{ Log } |(p_s/p_r)|^2 \tag{A.1}$$

where NR = Noise reduction across a panel (dB)

p_s = measured sound pressure at the source side (N/M^2)

p_r = Measured sound pressure at the receiver side (N/M^2).

For a plane wave with partial absorption on the receiver side, the noise reduction can be written by

$$NR = 10 \text{ Log } (1 + \tau/\alpha) \tag{A.2}$$

where τ = Panel transmission loss coefficient

α = Absorption coefficient of the Beranek tube.

The sound transmission loss of a multilayered panel is calculated from the pressure losses across individual layers. A typical multilayered panel is shown in Figure A.1. The transmission loss of a multilayered panel is obtained from

$$TL = 10 \text{ Log } (1/\tau) = 10 \text{ Log } |(p_1/p_t)|^2 \tag{A.3}$$

where TL = Transmission loss across the panel (dB)

τ = Transmission loss coefficient

p_1/p_t = Pressure ratio across the entire configuration in n layers

n = total number of layers in the panel.

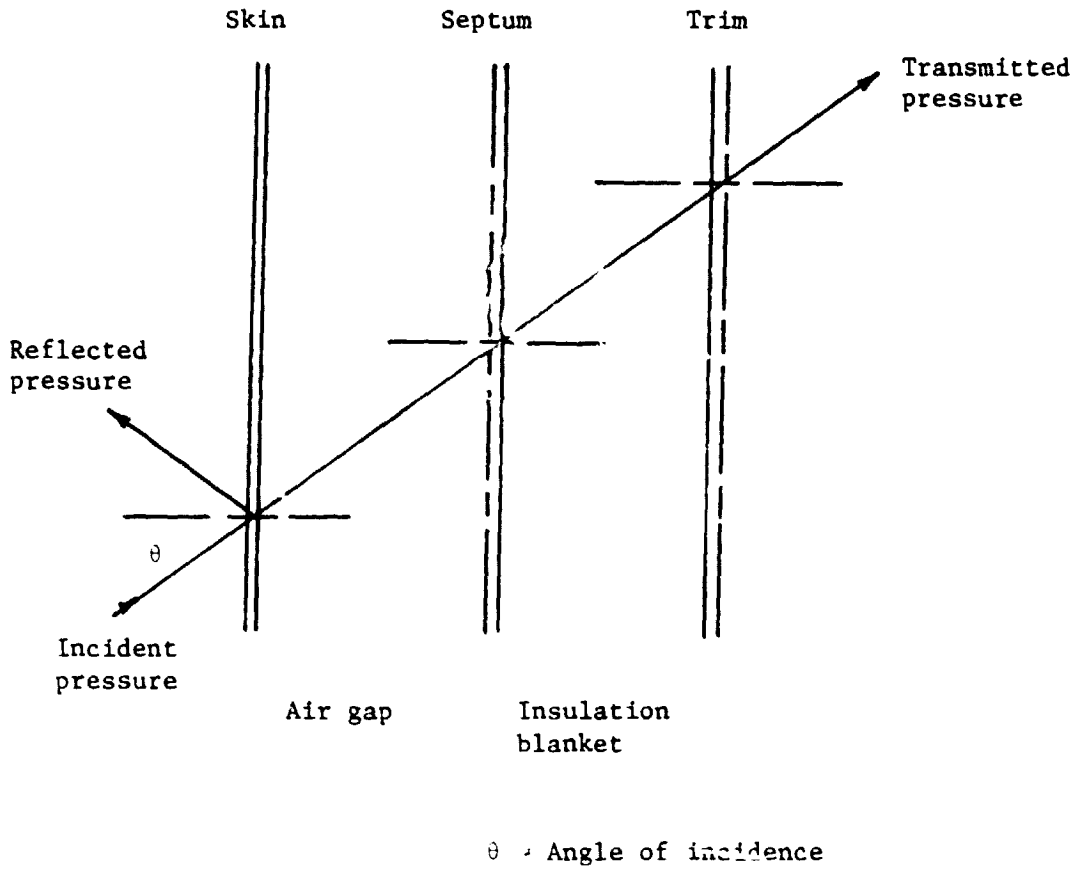

Figure A.1: Schematic Diagram of Multilayered Panel

Also the pressure ratio across the entire panel can be written in terms of the pressure ratio across individual layers:

$$(p_i/p_t)^2 = (\frac{p_i}{p_2} \cdot \frac{p_2}{p_3} \cdots \frac{p_k}{p_{k+1}} \cdots \frac{p_n}{p_t})^2$$

where $\frac{p_k}{p_{k+1}}$ = Pressure ratio across k in layers.

A typical sound treatment used in an aircraft is made of skin, air gaps, sound (and temperature) insulation, septa, and trim panel. Skin is s stiffened curved shell made from aluminum or composite panel. The sound insulation is a fiberglass pourous material usually enclosed in impermeable vinyl. Septa are very thin limp vinyl with very low surface mass density. The decorative interior trim panel varies widely from porous aluminum sheet with leather trim to Klegecell type panels with vinyl trim. A list of the generally used trim panels and the noise reduction characteristics of 18 x 18 inch specimens are detailed in a KU-FRL report (Reference 1). In addition, leaded vinyl sheets are also sometimes used as a lyaer to increase the sound transmission loss. Whenever the frame depth is greater than the insulation thickness, there is an air gap, which also has to be considered as a layer. The pressure ratio across each layer is calculated from the impedance of the layer and the impedance of the layers and the receiver cavity downstream of the layer under consideration (References 15 and 16). The test panels at the KU-FRL acoustic test facility simulate the actual aircraft panels. These panels have stiffened aluminum skin, air gap, fiberglass insulation, septa, and trim.

A.1.1 Multilayer Panel Characteristics

For a skin panel subjected to an obliquely incident sound wave with an airflow, the pressure ratio is obtained from (Reference 16)

$$\frac{p_I}{p_2} = \frac{1}{2}\left[1 + \frac{z_p \cos\theta_2}{z_2} + \frac{\rho_1 C_1 \cos\theta_2}{\cos\theta_1 (1 + M \sin\theta_1) z_2}\right.$$

where p_I = Incident pressure

p_2 = Transmitted pressure

Z_p = Characteristic impedance of skin panel

z_2 = Terminating impedance for the skin panel

θ_2 = Angle of incidence in Region 2

θ_1 = Incident angle of incidence

$\rho_1 C_1$ = Impedance of air on the source side

M = Mach number.

Equation (A.5) can be simplified when the external flow is not considered.

$$\frac{p_I}{p_2} = \frac{1}{2}\left[1 + \frac{Z_p \cos\theta_2}{z_2} + \frac{\rho_1 C_1 \cos\theta_2}{z_2 \cos\theta_1}\right] \qquad (A.6).$$

The impedance of a stiffened panel is modeled in the KU-FRL program in three ways:

a) The impe ance of a flat panel bounded by stiffeners and with in-plane stresses to simulate pressurization is defined by (Reference 16)

$$Z_p = \frac{\omega_n^2}{\omega} m\eta + \frac{\omega^3 D\eta}{C_1^4} \frac{\sin^4\theta}{(1 + M \sin\theta)^4} + j\left[\omega m - \frac{\omega_n^2 m}{\omega} - \frac{\omega_n^3 D}{C_1^4} \frac{\sin^4\theta}{(1 + M \sin\theta)^4}\right] \qquad (A.7)$$

where ω_n = Fundamental angular resonance frequency

$$= \frac{\pi}{(m)^{1/2}} \left[\left(\frac{P_{ax}}{a^2} + \frac{P_{cir}}{b^2} \right) + D\pi^2 \left(\frac{1}{a^2} + \frac{1}{b^2} \right)^2 \right]^{1/2} \quad \text{(A.8)}$$

η = Loss factor

D = Flexural rigidity $[Eh^3/12(1 - \nu^2)]$

C_1 = Speed of sound on the source side

θ = Angle of incidence

M = Mach number

P_{cir} = Axial load due to pressurization

P_{ax} = Circumferential load due to pressurization

m = Mass per unit area

E = Young's modulus of the skin

ν = Poisson's ratio

h = Skin thickness.

b) A hypothetical one-mode model (SDOF model) with the follcwing impedance is also used based on Reference 26:

$$Z_p = 2\zeta\omega_n + j\omega m\left[1 - \left(\frac{\omega_n}{\omega}\right)^2\right] \quad \text{(A.9)}$$

where ζ = Damping ratio

ω_n = Angular natural frequency

m = Mass per unit area

c) The third model used for skin impedance is derived from .mple mass law and is given by

$$Z_p = j\omega m \quad \text{(A.9a).}$$

A.1.2 Septum Characteristics

When an internal layer (leaded vinyl or vinyl) is present, the following equation is used to determine the pressure ratio across the layer:

$$p_i/p_{i+1} = z_i \cos\theta_{i+1}/z_{i+1} \tag{A.10}$$

where $z_i = Z_p + z_{i+1}$ (A.11)

$Z_p = j\omega m_i$ (A.12)

$\omega = 2\pi f$

m_i = mass per unit area of layer i

f = frequency

z_{i+1} = Terminating impedance for layer i, calculated from impedance downstream of layer i + 1.

The input impedance z_i is simply the sum of the layer impedance and the terminating impedance.

A.1.3 Air Gap or Porous Material Characteristics

The pressure ratio across an airspace or a soft porous blanket subjected to an obliquely incident ray is given by (References 16 and 17):

$$\frac{p_i}{p_{i+1}} = \frac{\cosh\left[bd\cos\phi + \coth^{-1}\left(\frac{z_{i+1}\cos\phi}{z_B}\right)\right]}{\cosh\left[\coth^{-1}\left(\frac{z_{i+1}\cos\phi}{z_B}\right)\right]} \tag{A.13}$$

where b = Complex propagation constant (calculated from equations and data in Reference 27 for porous blankets)

$b = j\omega c$ for air gap (A.14)

z_{i+1} = Termination impedance

Z_B = Characteristic impedance of the layer (calculated from Reference 33 for porous blanket)

$Z_B = \rho c$ for air gap.

The input impedance of the blanket is given by (Reference 16):

$$z_i = \frac{Z_B}{\cos\phi} \coth[bd\cos\phi + \coth^{-1}\frac{z_{i+1}\cos\phi}{Z_B}) \quad \text{(A.18)}.$$

A.1.4 Trim Panel Characteristics

The pressure ratio across the trim panel is similar to Equation A.9. Only the panel impedance is modified. Three impedance models are used. These are given by either Equation A.7, A.9, or A.12.

A.2 CALCULATION OF AVERAGE TRANSMISSION LOSS

From the characteristic impedance of each layer, the pressure ratio for that layer is calculated. The TL is calculated from Equation A.4 using these pressure ratios. The effect of random incidence angle is simulated over a range of incidence angles and averaged based on Reference 16 as

$$\bar{\tau} = \int_0^{\theta_1} z(\theta)\sin 2\theta d\theta.$$

The transmission loss equations for the frquency up to 5000 Hz are calculated and stored in a data file, which then can be plotted on the HP 7225B plotter using the plotter program written for this purpose.

APPENDIX B

DETAILS OF INTERIOR NOISE CONTROL PROGRAM

The interior noise control program developed at the KU-FRL acoustic research facility is a series of programs written in Fortran IV language on a Digital MINC-11 computer operating under an RT-11 system. This Fortran, also called PDP-11 Fortran, is an enhanced version of ANSI-66 Fortran (Refrence 48). The MINC-11 computer is a 16 bit minicomputer with 64 K byte memory. Due to the limitation in memory size, the main program has been divided into a series of small programs. Details of individual programs are given in the subsequent sections.

B.1 PROGRAM SHELM

Purpose: Calculation of sound transmission loss in a thin cylindrical shell (monocoque structure).

Based on: References 9 and 16.

Input: Data file: PNLxxx.DAT

Output: On line printer: frequency, transmission loss, and number of modes to converge.

On data file: frequency, transmission loss.

Notes: 1. All the outputs will be in correct format for entry into either TLPLOT or SUMTL programs.

2. This program calculates the impedance of the shell based on Reference 9. In addition to this model, another subroutine is also present. This is based

on Reference 11. In this routine the shell impedance is based on a matrix computation.

3. The subprograms needed to link are

   a. SHELM.OBJ

   b. SUBAM.OBJ

   c. 0:BESJ.OBJ

   d. 0:BESY.OBJ

   The executable file is called SHELM.SAV.

   For shell impedance based on Reference 11, the subprograms needed are

   a. SHELM.OBJ

   b. SUBAMI.OBJ

   c. 0:BESJ.OBJ

   d. 0:BESY.OBJ

   The executable file is called SHELMI.SAV.

B.2 PROGRAM SHELS

Purpose: Calculation of sound transmission loss in a thin stiffened cylindrical shell (smeared stiffness method).

Based on: References 10 and 16.

Input: PNLxxx.DAT

Output: On line printer: frequency, transmission loss, and number of modes required to converge.

On data file: frequency, transmission loss.

Notes: 1. All the outputs will be in correct format for entry into either PLOT or SUMTL programs.

2. This program calculates the impedance of the shell based on Reference 10.

3. The subprograms needed to link are

   a. SHELS.OBJ

   b. SUBA.OBJ

   c. SUBB.OBJ

   d. 0:BESJ.OBJ

   e. 0:BESY.OBJ

   The executable file is called SHELS.SAV.

B.3 PROGRAM SKINL

Purpose: Calculation of sound transmission loss of a skin panel with and without treatment.

Based on: References 16 and 17.

Input: Data File: PNLxxx.DAT

Output: On line printer: frequency, transmission loss of panel without any treatment, transmission loss of panel with treatment, and additional transmission loss due to the treatment.

Data file: frequency, TL_1, TL_2, TL_3

Notes: 1. The outputs in data file will be in correct format for TLPLOT or SUMTL programs.

2. This program has a small interactive part. This is used to vary the noise control treatment.

3. The files needed to link and run are

   a. SKINL.OBJ

   b. SKINLB.OBJ

   c. FUNC.OBJ

   The executable fine is called SKINL.SAV.

4. A slightly different version which calculates the panel impedance using Milulas' equation (Reference 17) is called SKINLI.SAV. The version TRIMTL.SAV has the modifications discussed in Section 2.6.

B.4 PROGRAM TLSI

Purpose: Calculation of the effect of individual noise control elements on the overall transmission loss of treated panels at selected frequencies.

Based on: References 16 and 17.

Input: Data file PNLxxx.DAT

Output: Data file (STL.DAT): value of the parameter that is being varied, transmission loss at selected frequencies.

Notes: 1. This program has no output on the line printer. The results are plotted using Program PLTSTL.SAV.

2. The parameters that are considered controllable are air gap, thickness, insulation thickness, septum surface density. The effect of each of these

C-2

parameters is studied by varying them from half to 2 times the nominal value input into the program.

3. The frequencies at which these effects are studied are 60, 100, 200, 500, 1000. These values can be changed.
4. The subprograms needed to compile are

   TLSI.OBJ

   SKINLB.OBJ

   FUNC.OBJ.
5. The executable file is called TLSI.SAV.

B.5 OTHER UTILITY PROGRAMS

In addition to the above programs, several utility programs have been written.

a. Program TLPLOT plots the results from SHELM, SHELS, SKINL, SKINLI, TRIMTL, SUMTL programs on the HP7225B digital plotter.

b. Program PLTSTL plots the results from TSLI program on the HP7225B digital plotter.

c. Program SUMTL calculates the transmission loss of treated structure based on the following equations (Reference 16):

$$TL_{\text{untreated structure}} = \text{Minimum}(TL_{\text{shell}}, TL_{\text{untreated panel}})$$

$$TL_{\text{added trestment}} = TL_{\text{treated panel}} - TL_{\text{untreated panel}}$$

$$TL_{\text{treated structure}} = TL_{\text{untreated structure}} + TL_{\text{added treatment}}$$

The inputs are the output data files from SHELM (or SHELMI or SHELS) program and SKINL (or SKINLI or TRIMTL) program.

The output data file is called TRSxxx.DAT, which can be plotted using TLPLOT program.

APPENDIX C

ACCELEROMETER MOUNTING

No references could be found concerning the process of mounting accelerometers. The accelerometer manuals showed only the relative merits of each type of mounting. The following methods for mounting with cement were adopted from the methods of strain gage installation detailed in Reference 49.

C.1 MOUNTING WITH CEMENT

C.1.1 Cleaning

a) Aluminum

1. Degrease with Chlorothene Nu.
2. Wet sand with 400 grit paper and Conditioner A.
3. Scrub with Conditioner A on cotton-tipped applicator.
4. Scrub with Neutralizer 5 on cotton-tipped applicator.

Do steps 1 through 4 on material, then on the accelerometer mounting stud.

b) Graphite and Kevlar

1. Degrease with Freon TF.
2. Dry sand with 400 grit paper to remove surface gloss.
3. Scrub clean with Freon TF on cotton-tipped applicator.
4. Scrub with Neutralizer 5 on cotton-tipped applicator.

Clean the accelerometer mounting stud as for aluminum.

C.1.2 Mounting

1. Lift brush cap out of catalyst bottle and wipe approximately 10 strokes against the lip of the bottle. Slide the brush over the accelerometer mounting base (do not stroke). Allow to dry at least one minute.
2. Apply less than a drop of cement (M-Bond 200) to the material (this will depend on the accelerometer size). The instructions call for one drop per square inch.
3. Immediately place the accelerometer in the desired position and press down and hold for two minutes or longer.

C.2 MOUNTING WITH BEE'S WAX

1. Clean the area on the panel with acetone.
2. Apply a small amount of wax to the base of the accelerometer (enough to cover the base).
3. Press the accelerometer onto the desired spot of the panel until there is a fairly thin layer of wax bonding the accelerometer to the panel. If this layer is too thick, extraneous losses will result.
4. Remove excess wax squeezed out from the accelerometer.

C.3 ACCELEROMETER CABLES

Extreme care must be taken when removing and connecting the cable to the accelerometer and to the SLM. Leaving the cable attached to

the accelerometer is recommended to minimize the chances of breaking the fragile cable ends.